Helsinki University of Technology Doctoral Theses in Materials and Earth Sciences
Espoo 2007 TKK-ME-DIS-6

THE CRYSTAL AND MAGNETIC MICROSTRUCTURE OF Ni-Mn-Ga ALLOYS

Doctoral Thesis

Ge Yanling 葛艳玲

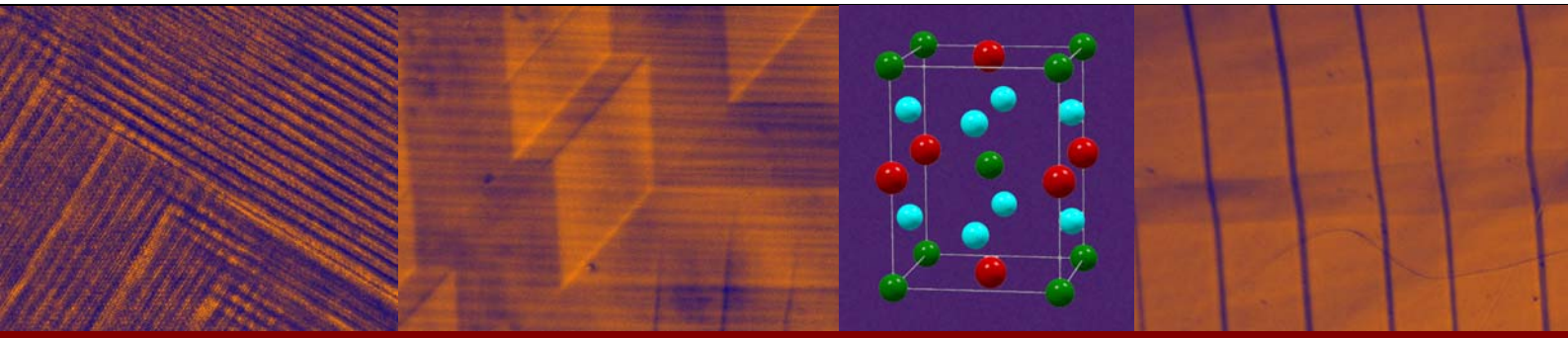

KK-ME-DIS series
Helsinki University of Technology
Department of Materials Science and Engineering
P.O. Box 6200
FIN-02015 TKK

Helsinki University of Technology Doctoral Theses in Materials and Earth Sciences
Espoo 2007 TKK-ME-DIS-6

THE CRYSTAL AND MAGNETIC MICROSTRUCTURE OF Ni-Mn-Ga ALLOYS

Doctoral Thesis

Yanling Ge

Dissertation for the degree of Doctor of Science in Technology to be presented with due permission of the Department of Materials Science and Engineering, Helsinki University of Technology for public examination and debate at Helsinki University of Technology (Espoo, Finland) on the 13th of April, 2007, at 12 o'clock noon.

Helsinki University of Technology
Department of Materials Science and Engineering
Laboratory of Materials Science

Teknillinen korkeakoulu
Materiaalitekniikan osasto
Materiaalitieteen laboratorio

Distribution:
Helsinki University of Technology
Laboratory of Materials Science
P.O. Box 6200
FIN-02015 TKK, Finland

Cover: Crystal and twin boundary structure of Ni-Mn-Ga alloy studied by X-ray and HRTEM, and 90 and 180° magnetic domains coupled with twins visualised by SEM and optical microscopy

ISBN 978-951-22-8661-4
ISBN 978-951-22-8662-1 (electronic)
ISSN 1795-0074

Picaset Oy
Helsinki 2007

ABSTRACT

The crystal structure and magnetic domain patterns of Ni-Mn-Ga alloys are studied in the present thesis work. The crystal structure of the martensitic phases in these alloys is highly dependent on the chemical composition. Single crystal X-ray diffraction shows that five-layered martensite is approximately a tetragonal phase with $c < a$, seven-layered martensite is orthorhombic and non-modulated martensite is a tetragonal type with $c > a$. Powder X-ray diffraction refinement suggests that five-layered martensite is a modulated structure with its basic structure having a monoclinic lattice, with the lattice parameter *a* being slightly different from the parameter *b*. Two-dimensional X-ray scattering distribution and electron diffraction confirmed that there are two shuffling systems with two modulation wave vectors. The interface, i.e. the macrotwin boundary, is formed between these two domains, which have a nearly orthogonal microtwin plane. This interface consists of two constituent elements, a step and a crossing. The layered martensite, which can be viewed as a periodic microtwin sequence, is not perfect; aperiodic plane faults and other-than nominal periodic microtwins are definitely present.

In a multi-variant martensite, each martensitic band consists of internal twins. The 180° magnetic domains arise from the major internal twin variant, which is observed both by Type I and Type II magnetic contrast with a scanning electron microscope. The minor internal twin variants show a zigzag pattern when the *c*-axis is out of plane. In a two-variant state sample, the 180° magnetic domains follow the *c*-axis in each twin variant and continue to the neighbouring twin variant by a 90° domain wall, which coincides with the twin boundary. In a single-variant state the 180° magnetic domains are parallel to the *c*-axis and run through the whole observed surface. Optical observation of the magnetic domain pattern reveals that there is a surface relief associated with the magnetic domains. This surface relief causes the (011) twins to appear as a zigzag pattern when projected on the (010) plane. Such magnetic domain associated surface relief is due to the less strained surface as compared to the bulk during the magnetic shape memory phenomenon.

In this thesis work it is also found that the application of an excitation voltage of 20-30kV and the Kα line for Ga are critical factors for obtaining a reliable chemical composition for Ni-Mn-Ga alloys using energy-dispersive spectrometer and wavelength-dispersive spectrometer analysis. It is discovered that there are two shuffling systems and the interface between them consists of step and crossing elements in five-layered martensite. It is revealed for the first time in Ni-Mn-Ga alloys that surface relief is associated with the magnetic domains. This provides a new opportunity to observe the magnetic domain patterns with an optical microscope.

Keywords:
Ni-Mn-Ga alloys, magnetic shape memory effect, martensitic transformation, magnetic domains, X-ray diffraction, high-resolution transmission electron microscopy, EDS analysis, WDS analysis, twin boundaries, microtwins

PREFACE

The work for the present thesis was carried out in the Laboratory of Materials Science at Helsinki University of Technology. The main part of this work was carried out in the Magnetic Shape Memory materials project during 1998-2003, which was supported by Tekes, the Finnish National Agency for Technology and Innovation, and the participating Finnish companies, Metso Paper Oy, Nokia Oyj – the Nokia Research Centre, Outokumpu Research Oy, ABB Corporate Research Oy, and AdaptaMat Ltd. The work was finalised with the support of a postgraduate scholarship from Helsinki University of Technology, a Chinese Government Award for Outstanding Self-financed Students from the China Scholarship Council, and a grant from Outokumpu Foundation.

First of all, many thanks to Prof. Veikko Lindroos for his help and support and for giving me the chance to work in this interesting field of magnetic shape memory alloys and start my thesis work. I would also like to thank Prof. Simo-Pekka Hannula for his help and supervision in my finishing this thesis work. I sincerely acknowledge Dr. Outi Söderberg for all her advice and encouragement, also outside the scientific field. I am grateful to Dr. Oleg Heczko and to Dr. Alexei Sozinov for their encouragement and helpful discussions. And I would like to thank Mrs. Marjatta Aav for her kindly help with almost everything and Mrs. Pirjo Korpiala for her help with sample preparation and many other things. I want to thank all the members of the HUT-MSM team and the staff members and the unforgettable students of the Laboratory of Materials Science.

Finally, I would like to thank my husband Zou Wei and my lovely daughter Zou Yulin for their love, support, and patience in helping me to finish this work.

Espoo 2006

Yanling Ge

LIST OF PUBLICATIONS

P1. *O. Söderberg, A. Sozinov, Y. Ge, S.-P. Hannula, V.K. Lindroos,* **Giant Magnetostrictive Materials**, In: Buschow J (ed.) Handbook of Magnetic Materials, Volume 16, Elsevier Science, Amsterdam, (2006),1-39.

P2. *Y. Ge, E. Heikinheimo, O. Söderberg, V.K. Lindroos,* **Microanalysis of a NiMnGa alloy**, Proceedings of Scandem 2002, 12-15 June 2002, Tampere, Finland, (2002), 120-121.

P3. *Y. Ge, O. Söderberg, N. Lanska, A. Sozinov, K. Ullakko and V.K. Lindroos,* **Crystal structure of three NiMnGa alloys in powder and bulk materials**, Journal de Physique IV, **112** (2003), 921-924.

P4. *Y. Ge, H. Jiang, A.Sozinov, O.Söderberg, N Lanska, J. Keränen E. I. Kauppinen, V.K. Lindroos S.-P. Hannula,* **Crystal structure and macrotwin interface of five-layered martensite in Ni-Mn-Ga magnetic shape memory alloy**, Materials Science & Engineering, **A 438–440** (2006), 961-964.

P5. *Y. Ge, O. Heczko, O. Söderberg, and V. K. Lindroos,* **Various magnetic domain structures in a Ni-Mn-Ga martensite exhibiting magnetic shape memory effect**, Journal of Applied Physics, **96** (2004), 2159-2163.

P6. *Y. Ge, O. Heczko, O. Söderberg and S.-P. Hannula,* **Direct optical observation of magnetic domains in Ni-Mn-Ga martensite**, Applied Physics Letters, **89** (2006), 082502/1-3.

P7. *Y. Ge, O. Heczko, O. Söderberg S.-P. Hannula,* **Magnetic domain evolution with applied field in a Ni-Mn-Ga magnetic shape memory alloy**, Scripta Materialia, **54** (2006), 2155-2160.

BRIEF DESCRIPTION OF THE PUBLICATIONS

The present thesis is based on the results of the publications mentioned above and appended to this thesis. The present work combines and analyses the main results of the individual publications, which, in summary, are as follows:

Publication 1, "*Giant Magnetostrictive Materials*", gives a review of magnetic shape memory alloys. The focus is on research work with Ni-Mn-Ga alloys, which includes the modelling of the behaviour of the giant magnetic field-induced strain, the phase transformation, the mechanical and magnetic properties, the implementation of martensite variant rearrangement in an applied magnetic field and the relevant parameters, and the outlook for promising magnetic shape memory materials. The summary suggests that understanding the twinning structure and magnetic behaviour is a key factor for the design of new active materials and improving the present ones.

Publication 2, "*Microanalysis of a NiMnGa alloy*", investigated the reliable microchemical analysis and homogeneity of a Ni-Mn-Ga alloy with the Wavelength-Dispersive Spectroscopy (WDS) and Energy-Dispersive Spectroscopy (EDS) methods. Reliable results at 20-30 kV were obtained by analysing a Ni-Mn-Ga alloy with the K_α line for Ga element with both WDS and EDS. The studied alloy was homogeneous on a micro-scale.

Publication 3, "*Crystal structure of three NiMnGa alloys in powder and bulk materials*"; three alloys with different martensitic structures were studied with X-ray diffraction in powder and bulk material. The alloy $Ni_{49.5}Mn_{28.6}Ga_{21.9}$ is a tetragonal phase with five-layered modulation. Its X-ray powder diffraction was in good agreement with single crystal diffraction. The crystal structure was determined with a modulation model by Rietveld powder diffraction refinement, and the refined basic structure is a monoclinic lattice. The $L2_1$ atomic order was well present in the powder diffraction pattern of the high-temperature phase. The other two high-temperature alloys showed a discrepancy between the powder diffraction pattern and the single crystal X-ray results, which was attributed to heavy deformation (long ball milling time) during the preparation of the powder.

Publication 4, "*Crystal structure and macrotwin interface of five-layered martensite in Ni-Mn-Ga magnetic shape memory alloy*"; X-ray diffraction showed that two shuffling systems exist in Ni-Mn-Ga alloys with five-layered martensite. Conventional transmission electron microscopy (TEM) studies confirmed their existence and also revealed the interface between them. A high-resolution transmission electron microscopy (HRTEM) study revealed the detailed structure of the interface, which consisted of two constituent elements. The other periodic micro-twin sequences, such as seven and ten, and aperiodic plane faults were mingled with the five-layered martensite.

Publication 5, "*Various magnetic domain structures in a Ni-Mn-Ga martensite exhibiting magnetic shape memory effect*"; the configuration of the magnetic domain patterns coupled together with the twin structures was studied in multi-variant, two-variant, and single-variant martensite by means of Type I and Type II magnetic contrast in a scanning electron microscope (SEM). In the multi-variant state, the martensite band consisted of internal twins, and the 180° magnetic domain patterns corresponded to the major internal twin variants. The minor twin variants displayed a zigzag pattern commensurate with the magnetic domains. In the two-variant state, the 180° domains were parallel

and anti-parallel to the *c*-axis in one twin variant and connected with the domains of the neighbouring twin variant by a 90° domain wall at the twin boundary.

Publication 6, "*Direct optical observation of magnetic domains in Ni-Mn-Ga martensite*", reported the direct optical observation of the magnetic domain patterns which are associated with a large surface relief in the martensitic phase of a $Ni_{49.5}Mn_{28.6}Ga_{21.9}$ alloy. The surface relief was due to the different straining of the surface and the bulk caused by the internal stresses associated with the magnetic shape memory effect. The surface relief is coherent at the (101) twin boundary. However, the surface relief causes the trace of the (011) twin boundary to form a zigzag pattern on the projection of the (010) plane.

Publication 7, "*Magnetic domain evolution with applied field in a Ni-Mn-Ga magnetic shape memory alloy*", investigated the evolution of the magnetic domain pattern together with a twinning structure under a magnetic field successively applied in two perpendicular directions by means of an optical microscope in a $Ni_{49.5}Mn_{28.6}Ga_{21.9}$ alloy. Both the magnetic domain pattern and the twin morphology changed to more complex ones after the magnetic field had been switched on and off three times. It suggested that each time the magnetic domain and martensitic twin nucleation take a unique path determined by the local imperfections. The optical visibility of the magnetic domain was caused by a surface relief associated with the 180° magnetic domain. The extent of the surface tilt that produced the observed zigzag pattern was estimated to be about 2° in the $Ni_{49.5}Mn_{28.6}Ga_{21.9}$ alloy that was studied.

AUTHOR'S CONTRIBUTION

The main part of this work was carried out in the HUT-MSM project. The author planned the research in Publications 2–7 and carried out most of the experiments presented in Publications 2, 3, and 5–7. The author is responsible for Publications 2–7 and wrote Section 3, as well as participating in the writing of the other chapters in Publication 1. All publications were discussed with co-authors. Prof. Veikko Lindroos was my supervisor till the end of 2003 and Prof. Simo-Pekka Hannula from 2004. Dr. Outi Söderberg carried out the DSC measurements and Dr. Erkki Heikinheimo helped with some of the scanning electron microscopy techniques. Dr. Oleg Heczko was responsible for the magnetic susceptibility measurements. Dr. Alexei Sozinov and Mrs. Nataliya Lanska carried out the single crystal X-ray measurements. The conventional transmission electron microscopy was carried out together with Dr. J. Keränen and the high-resolution transmission electron microscopy was carried out with the help of Dr. H. Jiang and Prof. E. I. Kauppinen.

SYMBOLS AND ABBREVIATIONS

Symbols

Al	aluminium, in the alloys as atomic-%
Ga	gallium, in the alloys as atomic-%
Mn	manganese, in the alloys as atomic-%
Ni_2MnGa	the stoichiometric Ni-Mn-Ga alloy
$Ni_{50.4}Mn_{29.3}Ga_{20.3}$	Ni-Mn-Ga alloy, where the numbers refer to the atomic percentages of the elements
Ni	nickel, in the alloys as atomic-%
W	tungsten
Oe, kOe	Oerstedt, kilo-Oerstedt, unit for magnetic field
T	Tesla, unit for magnetic field, $1T = 10^4$ Oe
$L2_1$	the ordering of Heusler alloy X_2YZ, where all of the atoms are located at the sites of a body-centered cubic lattice
B2’	the ordering of Heusler alloy X_2YZ, where X is order but Y and Z occupy their sites in the crystal lattice randomly
β	the high-temperature phase in noble metal alloys
5M	five-layered martensite in Ni-Mn-Ga and Ni-Mn-Al alloy
7M	seven-layered martensite in Ni-Mn-Ga alloy
7R	seven-layered martensite in Ni-Al alloy
14M	seven-layered martensite in Ni-Al alloy
a,b,c,β,γ	lattice parameters
a_c	a-axis length of cubic phase
b_t	b-axis length of tetragonal phase
c_t	c-axis length of tetragonal phase
ξ	the direction of TA_2 acoustic phonon branch
η_i	deformation parameter
λ	twin variant volume fraction
$Fm\bar{3}m$	Hermann-Mauguin symbol of space group No. 225
Fmmm	Hermann-Mauguin symbol of space group No. 69
I4/mmm	Hermann-Mauguin symbol of space group No. 139
P2/m	Hermann-Mauguin symbol of space group No. 10
x^j	the displacement of the j^{th} atom
A_n	the sinusoid coefficients
B_n	the cosinoid coefficients
q	modulation vector
Δ_j	the displacement of the j^{th} plane from its regular position
L	the periodicity of shuffling

K_α	K_α characteristic radiation, the emission is due to the transition of the atom of the K state to the L state
L_α	L_α characteristic radiation, the emission is due to the transition of the atom of the L state to the M state
μ_B	Bohr magneton $\mu_B = 0.927 \times 10^{-24}$ J/T
k_1	first magnetic anisotropy constant
k_2	second magnetic anisotropy constant
T_C	the Curie temperature
A_s	the reverse transformation start temperature (K)
A_f	the reverse transformation finish temperature (K)
M_s	the martensitic transformation start temperature (K)
M_f	the martensitic transformation finish temperature (K)
σ_{tw}	twinning stress
σ_m	magnetically induced stress
α	the angle between the projection of the (011) twin trace on the (010) plane and the [100] direction
β	the angle of the tilted surface
θ	the angle between the (011) and (010) planes
l	the original length on the surface
Δl	the difference of contraction of the bulk materials and the surface

Abbreviations

BEI	backscattered electron image
COMPO	composition mode in scanning electron microscope which is used in observing magnetic domains
DSC	differential scanning calorimeter
EDS	energy-dispersive spectrometer
f.c.c.	face-centred cubic
FFT	fast Fourier transformation
FSMA	ferromagnetic shape memory alloy
HRTEM	high-resolution transmission electron microscope
ICC	interference-contrast-colloid
MFIS	magnetic field-induced strain
MFM	magnetic force microscopy
MSM	magnetic shape memory
MSME	magnetic shape memory effect
OM	optical microscope
SAED	selected area electron diffraction
SEM	scanning electron microscope
TEM	transmission electron microscope

TOPO	topography mode in scanning electron microscope which is used in observing magnetic domains
WDS	wavelength dispersive spectrometer

TABLE OF CONTENTS

1. INTRODUCTION

Ni-Mn-Ga alloys are a new class of active materials, and show giant magnetic field-induced strain (MFIS). These materials are called magnetic shape memory (MSM) alloys, or ferromagnetic shape memory alloys (FSMAs). They are potential materials both for sensors and actuators. MFIS is based on the rearrangement of martensite twin variants under a magnetic field. The crystal structure basis for the occurrence of MFIS is high magnetic anisotropy of the martensitic phase, in which there exists only one easy magnetisation axis. Martensite variants that have their easy axis along the applied field direction grow at the expense of other variants by twin boundary motion driven by the applied field.

The high-temperature β phase is a cubic $L2_1$ structure in the near-stoichimetric Ni-Mn-Ga alloys. This parent phase, martensite phase transformation temperatures and the martensitic crystal structure are heavily dependent on the chemical composition. The Curie point (T_C) connected to the temperature region of magnetic transition from paramagnetic to ferromagnetic depends only weakly on it and the value of the T_C fluctuates around 370 K under a wide composition range. The martensitic phase can be a layered structure or a non-modulated tetragonal phase. MFIS is only observed in layered martensite: about 6 % MFIS is obtained in the five-layered structure and 10 % in the seven-layered one. The easy magnetisation axis always coincides with the shortest crystallographic axis of the modulated martensite while applying the coordinate system of the cubic phase. The coupling of the crystal structure and the magnetic domain structure is a prerequisite for MFIS.

In this thesis work the crystal structure is studied by means of X-ray and electron diffraction. The crystal structure and the twin boundaries are also studied with a conventional transmission electron microscope (TEM) and a high-resolution transmission electron microscope (HRTEM). It is postulated and confirmed that five-layered martensite consists of two sets of microtwins and an interface between two sets of microtwins inside one variant. The magnetic domain structure is visualised with a scanning electron microscope (SEM) and an optical microscope (OM). The configuration of the magnetic domain inside the twin variants and at the twin boundary is disclosed. The cause of the observed surface relief with the magnetic domains is postulated to be the interaction of the magnetic domains and twin boundary changes during magnetisation.

A brief literature review is provided in the following section. It will focus on the progress of the determination of the crystal structure and magnetic microstructure as well as the difficulties connected with this kind of study. An overall review of the magnetic shape memory alloy is present in the Publication P1. Section 2 explains the experimental methods used in this work. Section 3.1 gives a brief summary of the properties of Ni-Mn-Ga alloys. Section 3.2 outlines the results of the determination of the crystal structure and the microstructure of the twin boundaries. Section 3.3 presents the results of the magnetic domain patterns and the surface relief associated with it. Section 4 is a discussion of the martensitic structure and the model of the magnetic domain-accompanied surface relief. Section 5 provides the conclusions.

1.1 Crystal Structure

Prior to the discovery of the magnetic shape memory effect (MSME) in a Ni-Mn-Ga alloy in 1996 by Ullakko *et al.* [1], the stoichiometric Heusler Ni_2MnGa alloy was studied for its ferromagnetic properties and chemical ordering [2-6]. The magnetic properties of Ni_2MnGa were found to be dependent on the $L2_1$ order of the crystal structure, i. e. ferromagnetism is associated with the Mn-Mn distance [2,5]. The magnetic moment is about $4.17\mu_B$ mostly confined to the Mn atom but with a small moment ($< 0.3\mu_B$) associated with the Ni sites [3,4]. The Curie temperature of Ni_2MnGa is 376 K. This alloy undergoes a cubic-to-tetragonal structure transition upon cooling below 202 K [6]. This phase transition is a thermoelastic martensitic transformation, and thus Ni_2MnGa displays the shape memory effect and superelasticity [7]. Thermal martensite has a layered structure [4], and there are four additional spots along the [110]* direction in the X-ray diffraction pattern. Three successive stress-induced structural transitions were observed for specimens elongated in the $<100>_{cubic}$ direction or compressed in the $<110>_{cubic}$ direction [8-10]. Only one transition is stress-induced in compression along the $<100>_{cubic}$ axis. The first step stress-induced product has the same crystal structure as thermally induced martensite, which is called five-layered martensite because of the four extra diffraction spots in the X-Ray diffraction pattern. The successive stress-induced martensites are seven-layered and non-modulated martensite, respectively. Thermally induced seven-layered martensite has also been found in an off-stoichiometric $Ni_{52}Mn_{25}Ga_{23}$ [11].

1.1.1 Description of the crystal structure

The high-temperature phase was unambiguously determined by neutron and X-ray diffraction [4] as a Heusler structure with an $L2_1$ order. The lattice parameter of the stoichiometric alloy is around 5.82 Å, a value which is sensitive to chemical composition and heat treatment. The space group is 225, $Fm\bar{3}m$, where Mn atoms occupy the 4a position, Ga the 4b position and Ni the 8c position in the stoichiometric composition. This structure may also be described in terms of four interpenetrating face-centered-cubic (f.c.c) sublattices A, B, C, and D with the coordinates shown below [4].

A	B	C	D
$0\,0\,0$	$\frac{1}{4}\,\frac{1}{4}\,\frac{1}{4}$	$\frac{1}{2}\,\frac{1}{2}\,\frac{1}{2}$	$\frac{3}{4}\,\frac{3}{4}\,\frac{3}{4}$
$0\,\frac{1}{2}\,\frac{1}{2}$	$\frac{1}{4}\,\frac{3}{4}\,\frac{3}{4}$	$\frac{1}{2}\,0\,0$	$\frac{3}{4}\,\frac{1}{4}\,\frac{1}{4}$
$\frac{1}{2}\,0\,\frac{1}{2}$	$\frac{3}{4}\,\frac{1}{4}\,\frac{3}{4}$	$0\,\frac{1}{2}\,0$	$\frac{1}{4}\,\frac{3}{4}\,\frac{1}{4}$
$\frac{1}{2}\,\frac{1}{2}\,0$	$\frac{3}{4}\,\frac{3}{4}\,\frac{1}{4}$	$0\,0\,\frac{1}{2}$	$\frac{1}{4}\,\frac{1}{4}\,\frac{3}{4}$

If the $L2_1$ order is perfect, the Mn atoms will occupy the A sites and the Ga atoms the C sites. The B and D sites are occupied by the Ni atoms. If the Mn and Ga atoms randomly occupy the A and C sites, the structure becomes a B2' order. The temperature of a B2' to $L2_1$ transition is in the range from 800 K to 1000 K, depending on the chemical composition of the specimen [12]. With off-stoichiometric composition the degree of order is proportional to its chemical composition deviation from stoichiometric.

The martensitic structure was first described in the cubic coordinate system. The extra diffraction spots found along the (110) plane indicate that the (110) plane undergoes a periodic shuffling in the $[1\bar{1}0]$ direction, while every 5th (110) plane remains in its original position. The shuffling can be described by a modulation wave in which the martensite structure is refined by the coefficient of the modulation wave base on the X-ray diffraction data [10]. Shuffling means that transformation shear occurs periodically on the (110) plane and in the $\pm[1\bar{1}0]$ direction.

From the geometric viewpoint the martensitic transformation proceeds by transformation shear on the closed packed $\{110\}_{cubic}$ plane. There are two possibilities for the shear direction, the $\pm[1\bar{1}0]$ direction on each $\{110\}_{cubic}$ plane. Because the product phase inherits the atomic order of the parent phase, the martensite phase has a superlattice, as does the parent phase. In the cubic phase there are two kinds of atomic planes in the stack of the $(110)_{cubic}$ plane, shown in Figure 1(a). The five-layered martensite that results from shear on these $(110)_{cubic}$ planes, shown in Figure 1(b), consists of 10 atomic planes that are shifted relative to each other in the directions $\pm[1\bar{1}0]$ parallel to the closed packed plane. Similarly, the seven-layered martensite thus consists of 14 atomic planes [13].

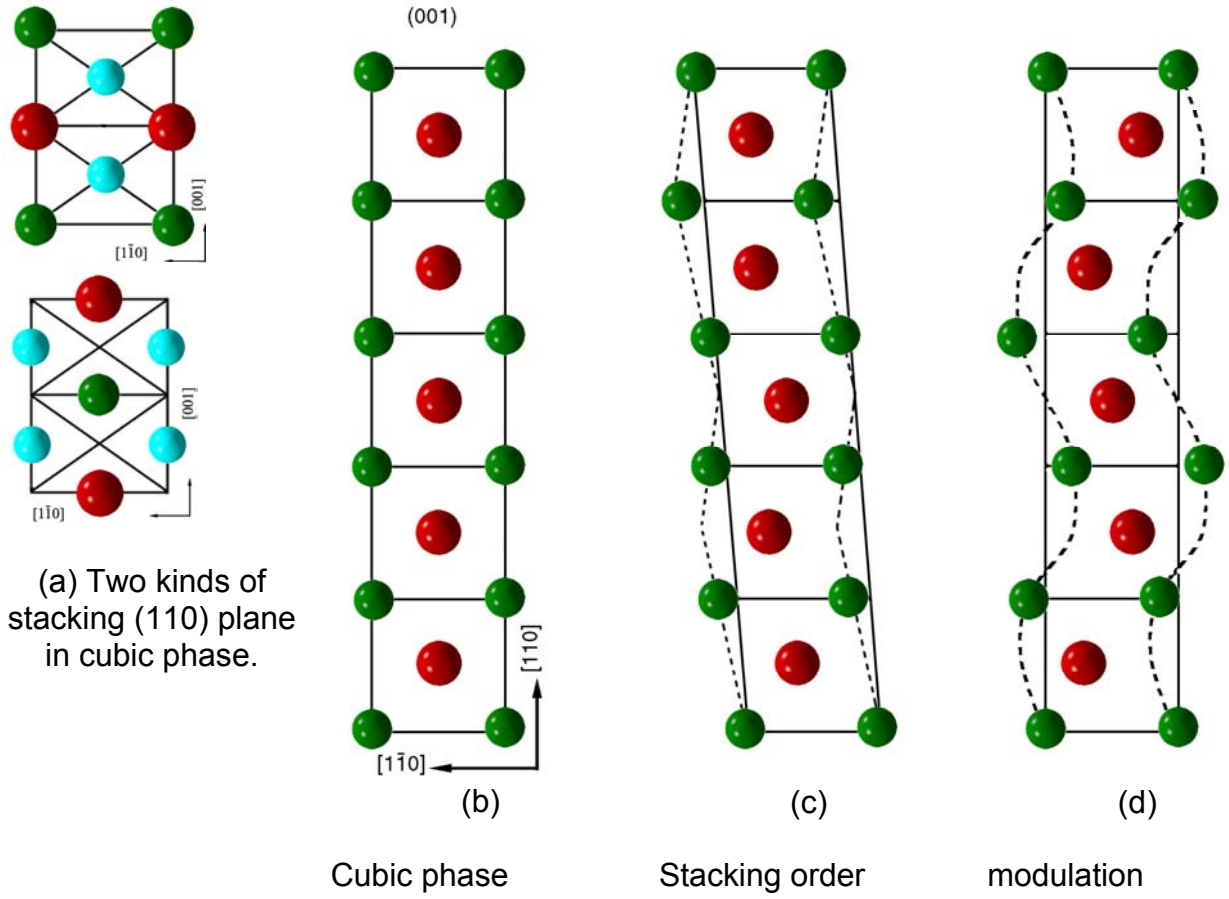

Figure 1. The illustration of two structure models and the original stacking order in the cubic phase.

The seven-layered martensite structure is well known in Ni-Al alloys. It has been named as $(5\bar{2})$ by Zhdanov notation and 7R by Ramsdell notation, in which R stands for rhombohedral symmetry. Later, the term 7R was replaced by 7M, in which M stands for monoclinic symmetry [14], because seven-layered martensite does not exhibit rhombohedral symmetry even if the ordering of the atoms

is disregarded. The abbreviation 14M is also seen in the literature [15] when the unit cell actually consists of 14 atomic planes after the new nomenclature for a long period stacking order martensitic structure as proposed by Otsuka *et al.* [16]. As a consequence, when five-layered martensite was found in the Ni-Mn-Al alloy it was named 10M by considering the $L2_1$ atomic ordering of the cubic phase [17]. Thus, in the case of Ni-Mn-Ga alloys, the abbreviations 5M or 10M for five-layered martensite and 7M or 14M for seven-layered martensite are all seen in the literature [18,19]. The problem of martensite nomenclature arises from the fact that martensite has a long period ordering structure and in order to describe the crystal structure precisely, the stacking order must be specified. Using M instead of R in addition to the number of layers is well accepted, because it reflects monoclinic symmetry. The diversity in the numbering of layers is due to the fact that the long-range atomic ordering doubles the number of atomic planes.

Furthermore, the naming problem also indicates two representations of the layered martensitic structure. The first one is the long-period stacking order structure, which is a well-known method to describe a close-packed layered martensitic structure. This method is based on uniform shear taking place on each basal plane, which is the $(110)_{cubic}$ plane for the β phase. The unit cell thus includes one period that usually contains several basal planes, such as 3, 6, 9, or 18. It is necessary to use Zhdanov notation to explicitly indicate the stacking sequence, such as $(5\bar{2})$ for seven-layered martensite. The uniform shear can easily be calculated according to the stacking order if the β angle of the monoclinic unit cell is known (which can usually be measured in a selected area electron diffraction (SAED) pattern) [13].

The second approach is to consider the layered structure as a one-dimensional modulation function superimposed onto the basic structure. The deviations of atoms from their ideal positions are defined by the modulation function. Thus, the introduction of a superspace group restores the crystal lattice periodicity. The modulation function can be described by Fourier series as:

$$x^j = \sum_n^{\infty} A_n \sin 2\pi nqj + \sum_n^{\infty} B_n \cos 2\pi nqj \qquad (1\text{-}1)$$

where x^j is the j^{th} atomic position and q is the modulation vector. Only a few of the lowest orders of the harmonic coefficients can be determined from the scattering experiment. In [10,11], sinusoid coefficients up to the third order are determined for five- and seven-layered structures.

The distinction between these two methods is that the stacking order model assumes uniform shear between two neighbouring atomic planes, which is the case only when considering the modulation function with the zero-order harmonic coefficients. Thus, the stacking sequence model is a simple example of a modulated structure and it is valid only for a commensurate modulated structure. Zheludev et al. found that the modulated martensitic structure of a near-stoichiometric Ni_2MnGa is an incommensurate one, in which the modulation is along the $(\xi\xi 0)$, $\xi = 0.43$ [20] by elastic neutron scattering. In this case, the modulation model is very suitable as a structure model. Figure 1 (c and d) gives the representation of two models which are derived from Figure 1(a) of the 10-layered (110)cubic plane.

From the modulated structure viewpoint, the basic structure of five-layered martensite is a tetragonal structure and that of the seven-layered martensite is orthorhombic. In the literature the tetragonal unit cell has two forms, one in the cubic coordinate system, i. e. the martensitic principle axes are derived from cubic axes, and the other with martensitic principle axes, the *a*- and *b*-axes,

derived from the {110} direction of the cubic phase. The unit cell in the first case is twice as large as in the second one. The first tetragonal structure can be described by the spacegroup Fmmm (No. 69) and the second one with the I4/mmm (No. 139). This is shown in Figure 2, which illustrates the unit cell of the $L2_1$ structure and two representations of the martensitic unit cell, the space groups I4/mmm and Fmmm, respectively. I4/mmm is a supergroup of Fmmm. From the crystallographic viewpoint the I4/mmm unit cell is more favourable because of its small volume. However, in practice the first description is directly related to the crystal lattice parameters affected by the magnetic field-induced strain, and the basic lattice vectors to the easy and hard magnetisation axes. Therefore, the Fmmm unit cell is commonly used in literature. And when the *a* axis is slightly different from the *b*-axis in the basic structure, the Fmmm group can still correctly describe the symmetry, although sometimes this small difference is indistinguishable within the tolerance of experimental error.

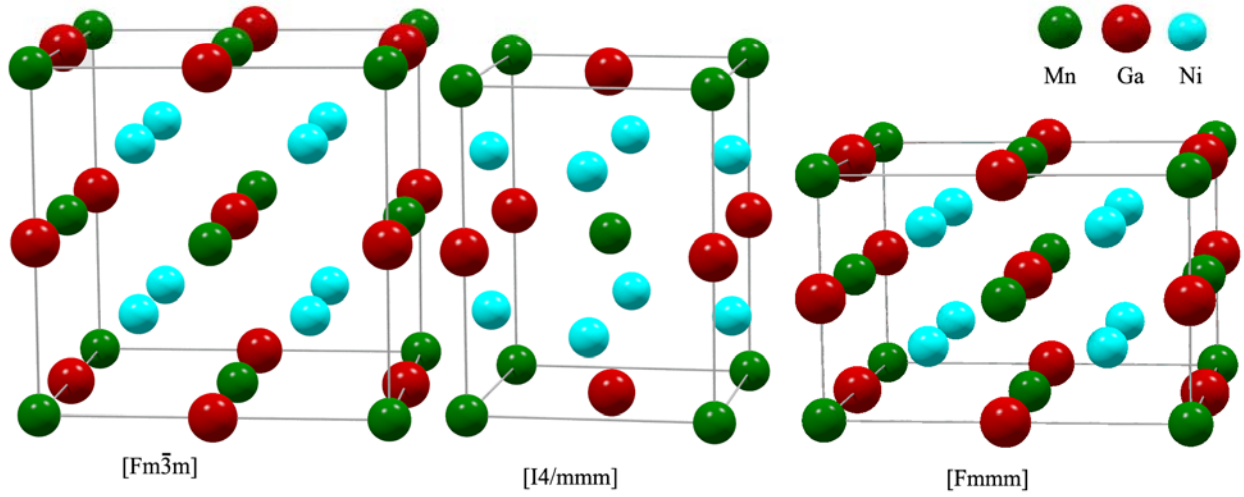

Figure 2. Heusler $L2_1$ structure and two kinds of martensitic unit cell.

1.1.2 Determination of the crystal structure

The determination of the crystal structure is mainly based on the diffraction data of neutron, X-ray, and electron diffraction. The X-ray atomic scattering factors of the elements Ni, Mn, and Ga are close to each other, but in neutron scattering the scattering lengths are very different and, therefore, neutron scattering can give more information about the chemical and magnetic ordering. The earlier crystal structure studies focused on the identification of the modulation periodicity by detecting character superlattice reflection [8,10,11,18,21,22]. Wedel et al. were the first to try to determine the crystal symmetry. They suggested the tetragonal (I4/mmm) and orthorhombic (Fmmm) structure models to describe martensitic structure [23]. Later Pons et al. analysed the electron diffraction data of five- and seven-layered martensite using both the modulation model and the stacking order model [19]. Here, $(3\bar{2})$ for five-layered martensite and $(5\bar{2})$ for seven-layered martensite gave good agreement with the intensities of the electron diffraction. They also determined a 10-layered martensite by the stacking order model as $(5\bar{5})$. They discussed these two descriptions from the physical point of view. Five-layered martensite is more suited to being described by the modulation structure because there usually exists a $(\xi\xi 0)$ TA_2-phonon branch softening at $\xi = 1/3$ or even a micromodulated premartensitic phase. Seven-layered martensite can be considered as an adaptive phase, i. e. a microtwinned tetragonal phase with a fixed periodicity. They also point out that the β

angle is critical for the determination of the structure model for five-layered martensite [19]. The modulation model should give the β angle as 90°, and apparently with the $(3\bar{2})$ stacking sequence the β angle deviates from 90°. This argument is based on the assumption that the basic structure is precisely determined as tetragonal: if the basic structure is slightly orthorhombic or monoclinic, the argument is not valid any more. The fine scale structure has also been studied by means of high-resolution transmission electron microscopy, in which the stacking sequence seems quite apparent [24].

Precursor phenomena, i.e. pretransitional effects, in shape memory alloys are associated with incipiently unstable acoustic modes related to the actual transition path [25]. It is found that the softening of the ($\xi\xi$0) TA_2-phonon branch occurs in a wide variety of Ni-Mn-Ga crystals, with martensitic transformation from far below room temperature to near the Curie temperature [26-29]. Only the softening width becomes larger with the martensitic transformation temperature increasing. These results reveal that the softening mode is not only relevant to five-layered martensite. The premartensitic transformation vanishes at the compositions in which intermartensitic transformation occurs, i.e. five-layered martensite changes to seven-layered or anther type of martensite. This may indicate that the softening mode gives rise to intermartensitic transformation, which is similarly to premartensitic transformation [30]. Indeed, a premartensite phase is found ahead of seven-layered martensite [31]. However, seven-layered martensite was mistaken for five-layered martensite in [32], even though its X-ray powder diffraction pattern is similar to seven-layered martensite, as in [19, P3].

1.2 Magnetic shape memory effect

Ni-Mn-Ga alloys may show ferromagnetic parent and martensitic phases at different temperatures. This makes it possible that the magnetic field is the driving force for shape change, in addition to external stress and temperature. The first observed magnetic field-induced strain in the martensitic phase was 0.2% [1]. This behaviour is also called the magnetic shape memory effect, as the original shape can be restored either by a field, heating, or stress. The observed strain arises from the twin variant rearrangement and is similar to that obtained by stress detwinning. Thus, the maximum strain can be expected with the change from one single variant to another. In a general case after the thermally induced phase transformation, martensites form a kind of self-accommodation multi-variant pattern to minimise transformation strain. By increasing the volume fraction of the preferred twin variant, higher value MSME has been reported, 0.32% [33], 4% [34,35], 5.1% [36], 6% [37] for five-layered martensite. Later, a giant magnetic field-induced strain of about 9.5% was reported for a seven-layered martensite [38]. The maximum MSME is limited by the martensitic lattice parameter, i. e. (1-c/a). Here, c and a are the basic lattice parameters of the Fmmm unit cell. This limit for five-layered martensite is around 6% and for seven-layered martensite around 10%.

It can be concluded from magnetisation curves that the high-temperature parent phase has weak magnetic anisotropy, while the martensitic phase possesses strong magnetic anisotropy [4]. Tickle et al. [35] measured the magnetisation curve of the cubic parent phase at different temperatures, and the results show that in this phase {100} is the easy axis of magnetization with anisotropy constant of an order of 10^3 J/m^3. In modulated martensite, there exists only one easy axis, which is the crystallographic c-axis of the Fmmm unit cell [35]. In a near-stoichiometric sample a value of 2.45

$\times 10^5$ J/m^3 is reported at a temperature of 256 K [35]. Many different values of the magnetic anisotropy constant of the martensitic phase have been presented in the literature [35,39-42]. This is due to the fact that the magnetic anisotropy constant is dependent on the composition of the alloy and temperature [43,44,46]. In [45], the magnetic anisotropy constants at room temperature were reported for five-layered martensite as $k_1 = 1.65 \times 10^5$ J/m^3 (k_2 negligible), for seven-layered martensite as $k_1 = 1.7 \times 10^5$ J/m^3 and $k_2 = 0.9 \times 10^5$ J/m^3 referring to the hard and mid-hard magnetisation axes, and for non-modulated martensite as $k_1 = -2.3 \times 10^5$ J/m^3 and $k_2 = 0.55 \times 10^5$ J/m^3.

1.3 Magnetic Domain Structure

The magnetic domain structure of martensite is crucial to an understanding of the mechanism of MSME and it is also a prerequisite for modelling this magneto-mechanical behaviour [1,34,42,47-49]. The first observations of magnetic domain structure were made by magnetic force microscopy (MFM) [34], which revealed a hierarchical domain structure with a herring-bone pattern, i.e. the 180° domains formed in each martensite variant. The same pattern was observed later by the Bitter pattern [50] and with magneto-optical indicator film imaging [42,51,52]. The magnetic domain width that was observed was in the range of several microns up to dozens of microns. A similar pattern was also observed with Lorentz microscopy, but the domain width here was 300 nm [53]. Pan et al. studied the evolution of this kind of pattern under an applied field by MFM [54]. The application of a small field (1-2 kOe) evolves this pattern to a firtree pattern meeting at the twin boundaries. The application of an intermediate field (4-5 kOe) in the easy direction of one twin variant caused the magnetisation vector of the neighbouring twin variants to rotate a little and the firtree pattern to localise at the twin boundaries. With larger fields (8-9 kOe), the magnetisation vector that was previously orthogonal to the field will rotate in the field direction and eliminate domain structure within a variant, so each twin band coincides with one magnetic domain.

In a surface with a magnetisation vector out of plane a labyrinth pattern [51] or a patch-like pattern [54] can be observed. Chopra et al. [55] found a fine ripple domain pattern superimposed with twin variants under a 400 Oe magnetic field by means of Interference-Contrast-Colloid (ICC) technique and this pattern did not change with the increase of one twin variant width when the field rose to 1800 Oe. With the use of the same technique the in situ observation of phase transformation showed that the 180° magnetic domain forms a zigzag pattern in twinned martensite with a well-defined periodicity of 25-30 μm [56].

The magnetic domain structure has been widely studied by means of TEM in thin foil specimens. The magnetic domain structure in the parent phase studied by means of the Lorentz microscopy [57] indicates long 180° domain walls with arrays of 71° domain walls in between in a (001) plane. The 71° domains follow the {111} axis of the cubic phase. The 180° domain walls show a cross-tie domain wall. Notably it was found that the domain pattern does not change simultaneously with the martensitic transformation. The evolution of the magnetic domain structure with temperature was also studied by Park et al. with Lorentz microscopy [58]. They reported in the parent phase large plate-like domains exceeding 1 μm at the edge and distinctive stripe domains in the inside area. Upon cooling, the stripe domains developed further, and before martensitic transformation they bent into a maze domain pattern. The premartensitic phase had the same domain pattern as the parent

phase. On cooling further, the stripe domains disappeared when the martensitic phase was formed. The domain walls coincided with the twin boundaries and there was also an area of additional domain walls across the twin boundaries, resulting in the division of each twin band into finer magnetic domains. Tsuchiya et al. [31] found out that the stripe domain is developed from a larger plate domain about 3 μm wide, just near the martensitic transformation temperature. This stripe domain pattern extends further upon cooling, while the large domain remains near the edge area. They also observed the stripe domain in the parent phase and speculated that it resulted from the demagnetisation field of the thin foil.

The magnetic domain structure observed by Lorentz TEM in thin film shows a similar domain pattern to the bulk materials to a certain extent: domain walls crossing twin boundaries cause one twin plate to have several small domains and twin boundaries also correspond to the domain walls [59]. In two other studies it has been shown that the film has a strong out-of-plane magnetic component and it indicates that strong anisotropy overcomes the demagnetisation field [60,61]. In [61], a maze pattern is observed and the domain width depends on the thickness of the film.

1.4 The aim of the present work

To summarise to the review of literature discussed above, the crystal structure of the martensitic phase of Ni-Mn-Ga martensite still lacks of some details regarding the lattice symmetry and atom positions, as well as the microstructure of the twin boundaries, even for the well-studied 5M martensite. Additionally, reports on the magnetic domain patterns show that their variety and their relationship to the twinning structure are not well understood yet. This work aims to investigate the crystal structure of Ni-Mn-Ga martensite by means of X-ray diffraction and electron diffraction together with HRTEM and image magnetic domain patterns in different martensite variant configurations in order to add detail to the understanding of the crystal and magnetic microstructure.

2. EXPERIMENTAL METHODS

Various Ni-Mn-Ga alloys were used in this study. The alloys $Ni_{50.4}Mn_{29.3}Ga_{20.3}$ [P2], $Ni_{50.4}Mn_{29.6}Ga_{20.0}$ [P2], $Ni_{52.6}Mn_{26.7}Ga_{20.7}$ [P3], and, $Ni_{48.9}Mn_{30.8}Ga_{20.3}$ [P4,P5] were manufactured in the Outokumpu Research Centre, Finland. The ingots of $Ni_{49.5}Mn_{28.6}Ga_{21.9}$ [P3,P4,P6,P7] and $Ni_{48.4}Mn_{31.3}Ga_{20.3}$ [P3] were produced at AdaptaMat Ltd. All the crystals were produced using a modified Bridgman method. The alloy $Ni_{48.9}Mn_{30.8}Ga_{20.3}$ [P4,P5] was homogenised at 1273 K for 48 h and thereafter annealed at 1073 K for 72 h. The alloys $Ni_{50.4}Mn_{29.3}Ga_{20.3}$ [P2], $Ni_{50.4}Mn_{29.6}Ga_{20.0}$ [P2], $Ni_{50.6}Mn_{26.7}Ga_{20.7}$ [P3] and $Ni_{49.5}Mn_{28.6}Ga_{21.9}$ [P3,P4,P6,P7] were homogenised at 1273 K for 72 h and thereafter annealed at 1073 K for 48 h. All these heat treatments were carried out by putting the samples into vacuum quartz ampoules. The correctly oriented specimens for the further studies were cut from the ingots by spark cutting and with a slow-speed diamond saw, ground with wet papers, and electro-polished using a 25% nitric acid ethanol solution either at ambient temperature or 273 K. The powder specimens were prepared by iron ball milling in an argon atmosphere containing approximately 1% hydrogen. The chemical

composition of the specimens was analysed by Wavelength-Dispersive Spectrometer (WDS) [P2] and Energy-Dispersive Spectrometer (EDS) in [P2,P3,P4,P5,P7,P6]. The reliability of the EDS results is verified by the WDS results [P2]. The EDS and WDS are attached to a W-cathode LEO-1450 scanning electron microscope. The crystal structure was investigated with X-ray diffraction and electron diffraction. The X-ray powder diffraction studies were carried out with a Philips diffractometer PW1710 with Cu-K_α radiation and the single crystal diffraction studies with a Philips X'pert-MRD with Co-K_α radiation [P3,P4]. The conventional transmission electron microscopy was carried out with a JEOL 2010 [P4], and the high-resolution electron transmission microscopy with a Philips CM-200FEG [P4]. The martensitic transformation temperature was characterised by the differential scanning calorimeter (DSC) of a Linkam-600 DSC. The Curie point was measured with a lab-constructed ac magnetic susceptibility instrument. The Type I and Type II magnetic contrasts in SEM were utilised to image magnetic domain structure [P5]. An optical microscope, a Leica DM RX, was used to study the magnetic domain-associated surface relief. For the details of the experimental equipment and procedures, see also [62].

3. SUMMARY OF RESULTS

A comprehensive literature review on magnetostrictive materials is presented in [P1]. The magnetic shape memory alloys are compared with other active materials, with the emphasis being placed on Ni-Mn-Ga alloys.

3.1 The properties of Ni-Mn-Ga alloys

In the off-stoichiometric Ni-Mn-Ga alloy the martensitic transformation and martensitic crystal structure are highly dependent on composition. The first-principles numerical calculations reveal the microscopic origin of the lattice instabilities and phase transformations. The macroscopic model of MFIS behaviour requires the twinning stress (σ_{tw}) to be below or close to the magnetically induced stress (σ_m), when taking into account the Zeeman energy, magnetic anisotropy energy, and magnetostatic energy. In reality the twinning stress, σ_{tw}, which is needed for the variant reorientation can be less than 1 MPa for five-layered martensite, close to 1 MPa for the seven-layered one, and at least 6 MPa for the non-modulated one.

The saturation magnetisation of ferromagnetic martensite in the Ni-Mn-Ga system depends on composition and temperature. The easy axis of magnetization is the crystallographic shortest *c*-axis in the five- and seven-layered martensites. In non-modulated martensite the long *c*-axis is the hard axis of magnetisation and there is an easy plane of magnetisation.

The large strain of about 6% of five-layered martensite can be obtained under a constant stress without the application of a magnetic field. This appears as a stress plateau in the stress-strain curve and the strain remains after unloading. When the same kind of material is mechanically deformed at a stress above 2.5-3 MPa in the orthogonal magnetic field, it behaves pseudo-elastically and the obtained shape change recovers totally in unloading. This spring-like behaviour is a prerequisite for the dynamic activation and it can be obtained when the triggering value of the magnetic field is

exceeded. The applied stress affects the obtainable MFIS and it should be less than 2.5-3 MPa. The MFIS value increases with decreasing compressive stress and the full MFIS is achieved when the stress is zero. During the dynamic actuation of Ni-Mn-Ga elements, an axial movement is usually applied, even though bending would also be possible. Sinlge Ni-Mn-Ga crystals have been used for the actuation of 2–4% strains with frequencies decreasing with the generated stroke.

The MSME is limited by the phase transformations and affected by the temperature dependence of the twinning stress, the tetragonality of the lattice and the magnetic anisotropy. The search for possible new MSM materials is focused on alloys with a thermally formed or stress-induced ferromagnetic thermoelastic martensite phase. The martensite should have extremely mobile twin boundaries. High magnetocrystalline anisotropy and high saturation magnetisation are also desirable properties.

3.2 Chemical composition, crystal structure, and twins

The martensitic transformation temperature of Ni-Mn-Ga alloys is heavily dependent on their chemical composition. In general, the transformation temperature increases with the electron-to-atom concentration (e/a); see Fig. 3.1 in [P1]. Here, it can also be seen that the temperature values are widely spread and cannot fit a simple linear relation, as suggested in some literature [6,64]. Possible reasons for this are that the chemical compositions are measured by different methods with different degrees of accuracy and/or the specimens have not been quite homogenous. An investigation of the reliability of the EDS results is reported in [P2]. When the applied electron voltage is 15 kV the data are quite spread both for EDS and WDS with the Ga K_α line and L_α line, respectively. At 20–30 kV, the EDS and WDS results have a good agreement for Ga K_α line. However, the Ga L_α line should not be used in WDS or in EDS analysis as it causes considerable deviation in the amount of Ga.

The five-layered martensitic crystal structure and its twin structure were investigated in two Ni-Mn-Ga alloys [P3,P4]. Their chemical compositions and phase transformation temperatures are given in Table 1.

As can be seen from Table 1, the phase transformation temperatures of the ternary powder specimens are quite close to the bulk materials. The powder made from the $Ni_{52.6}Mn_{26.7}Ga_{20.7}$ alloy was affected by Fe contamination from the long iron ball milling, resulting in a quaternary material with 1.4 at% Fe alloying. This is the cause of the clear difference between the transformation temperatures of these two materials.

The X-ray powder diffraction measurements of the powders were carried out at different temperatures, but the bulk material was studied only at ambient temperature by means of X'pert-MRD. Figure 3 shows the X-ray powder diffraction of the parent phase and the martensitic phase measured at 324 K and 298 K, respectively. The atomic scattering factors of the elements Ni, Mn, and Ga are quite close to each other, and therefore, the second neighbour order may not be visible in X-ray diffraction. However, in Figure 3(a) the peaks related to the second neighbour order are clearly present, i.e. the Bragg peaks (111), (311), and (331). The parent phase is indeed an ordered $L2_1$ structure. The crystal structure of the parent phase is refined with the Rietveld method on the basis of the powder diffraction pattern of Figure 3(a). The resulted lattice parameter is a = 5.837 Å.

Table 1. Chemical compositions and phase transformation temperatures of the alloys studied.

Alloy	M_s (K)	M_f (k)	A_s (K)	A_f (K)	T_C (K)
$Ni_{49.5}Mn_{28.6}Ga_{21.9}$ Bulk [P3,P4,P6,P7]	305.8	299.8	314.4	318.8	376.0
$Ni_{49.4}Mn_{28.8}Ga_{21.8}$ Powder [P3]	305.0	300.1	312.9	319.8	368.0
$Ni_{48.4}Mn_{31.3}Ga_{20.3}$ Bulk [P3]	354.0	347.4	356.0	363.2	363.0
$Ni_{48.4}Mn_{31.8}Ga_{19.8}$ Powder [P3]	354.2	346.5	354.1	360.6	362.0
$Ni_{52.6}Mn_{26.7}Ga_{20.7}$ Bulk [P3]	465.0	459.0	468.0	476.0	371.0
$Ni_{52.2}Mn_{25.6}Ga_{20.8}Fe_{1.4}$ Powder	423.0	383.0	393.0	428.0	352.0
$Ni_{48.9}Mn_{30.8}Ga_{20.3}$ Bulk [P4,P5]	324.0	321.0	332.0	335.0	370.0

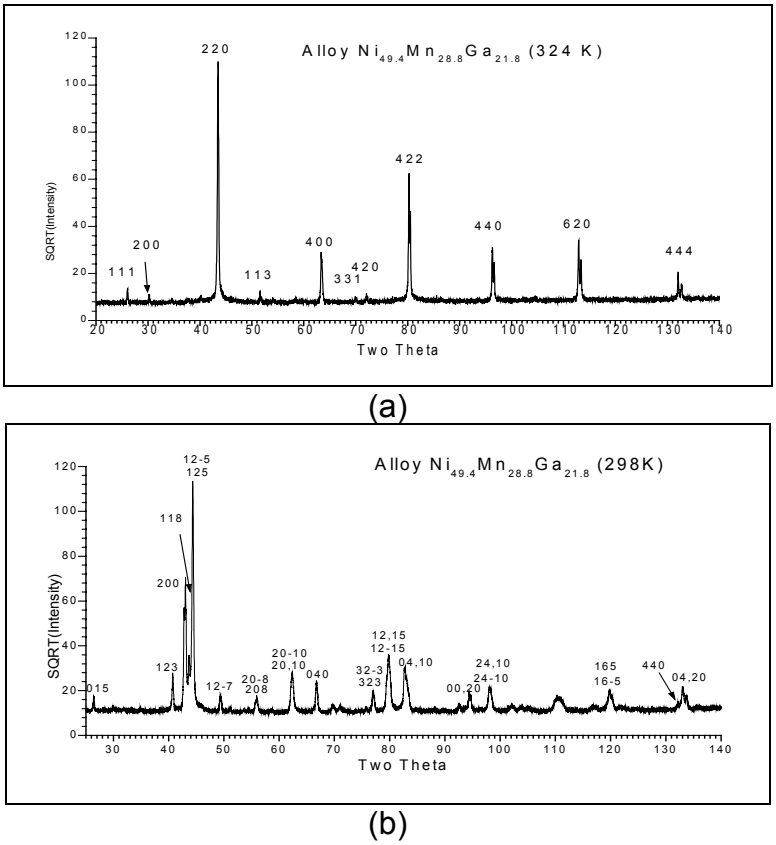

Figure 3. X-ray powder diffraction of the $Ni_{49.4}Mn_{28.8}Ga_{21.8}$ alloy. (a) Parent phase measured at 324 K; (b) Martensitic phase measured at 298 K [P3].

This is in good accordance with the value of (5.82 Å) given in [3] for the stoichiometric alloy, considering the difference in the chemical composition.

The martensite lattice parameters of the bulk material measured by a single crystal X-ray diffraction are $a = b = 5.95$ Å and $c = 5.61$ Å in the cubic coordinate system. The Rietveld refinement method is used to investigate the X-ray powder diffraction pattern of the martensitic structure; see Figure 3(b). Five-layered martensite is treated as a commensurate modulated structure. The modulation wave function is adapted from [11], in which only the sinusoidal part is taken into account, i.e.:

$$\Delta_j = \mathrm{A}_1 \sin 2\pi j / L + \mathrm{A}_2 \sin 4\pi j / L + \mathrm{A}_3 \sin 6\pi j / L \qquad (3\text{-}1)$$

where Δ_j is the displacement of the j^{th} plane from its regular position in the shuffling direction, and L is the periodicity of shuffling. The coefficients are $A_1 = -0.06$, $A_2 = 0.002$, and $A_3 = -0.007$. The basic structure is a tetragonal lattice with I4/mmm symmetry. The resulting big unit cell, which includes one period shuffling, fits the space group P2/m. The refined structure is a monoclinic cell and the lattice parameters are $a = 4.219$ Å, $b = 5.600$ Å, $c = 20.977$ Å, and $\beta = 90.2°$. The corresponding unit cell in the cubic coordinate system is also monoclinic with $a = 5.96$ Å, $b = 5.94$ Å, $c = 5.60$ Å, and $\gamma = 90.3°$.

The fact that refinement by the modulation model gives a β angle different from 90° for five-layered martensite suggests that this angle cannot be used to distinguish the modulation model and stacking order model. Therefore, the β angle deviation from 90° is directly ascribed to the monoclinic basic structure. The atomic simulation of the modulation structure shows that the Ni, Mn, and Ga atoms are displaced in different directions, and it indicates that displacement is not limited to the (110) plane [65]. By adapting the monoclinic basic structure, it is still possible to use the stacking order model to describe this lattice, but the stacking order model clearly cannot take this kind of displacement into account.

The $Ni_{48.4}Mn_{31.3}Ga_{20.3}$ alloy has its martensitic transformation temperature slightly below the Curie temperature. Single crystal X-ray diffraction shows that the crystal structure of the bulk material is a mixture of seven-layered martensite and non-modulated tetragonal martensitic phases. The measured lattice parameters for these two phases in the cubic coordinate system are $a = 6.21$ Å, $b = 5.80$ Å, $c = 5.50$ Å, and $a = b = 5.55$ Å, $c = 6.57$ Å, respectively. The X-ray powder diffraction shows quite a complicated pattern. The main reflection can be fitted to an orthorhombic lattice, which corresponds to the basic structure of seven-layered martensite, but the tetragonal phase cannot be identified from the heavily overlapping peaks. The comparison between the experimental data and theoretical calculations is shown in Figure 4 (a).

The bulk alloy $Ni_{52.6}Mn_{26.7}Ga_{20.7}$ has a simple non-modulated tetragonal martensitic structure with $c > a$. The phase transformation temperature is just above the Curie temperature. Single crystal X-ray diffraction showed that the lattice parameters are $a = b = 5.44$ Å, and $c = 6.64$ Å. In the powder specimen, 1.4 at% Fe is present, possibly because of the long duration of the iron ball milling during the specimen preparation. The X-ray diffraction of the powder diffraction is not a simple tetragonal phase but most of the peaks definitely fit seven-layered martensite, as shown in Figure 4(b).

The time for preparing the powder sample of five-layered martensite is only around 30 minutes, but for the seven-layered one it is 2 hours and for the non-modulated tetragonal phases over 6 hours. This may be due to the fact that seven-layered and non-modulated tetragonal martensites possess

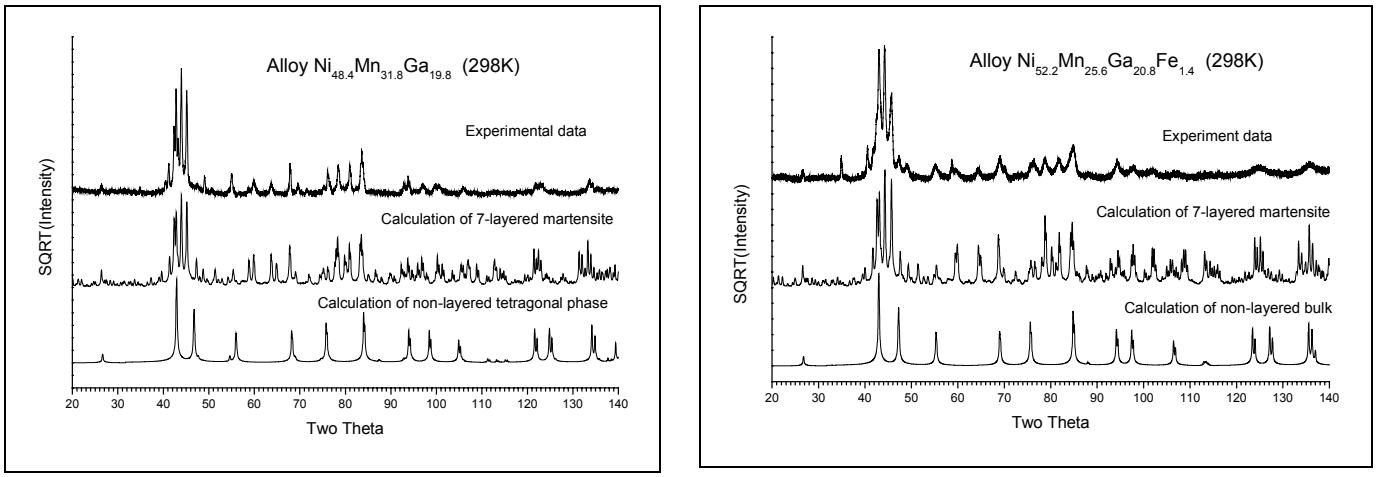

Figure 4. X-ray powder diffraction patterns of (a) the $Ni_{48.4}Mn_{31.8}Ga_{19.8}$ alloy and (b) the $Ni_{52.2}Mn_{25.6}Ga_{20.8}Fe_{1.4}$ alloy [P3].

dramatically different mechanical properties from those of the five-layered one [66]. The crystal structure controversy between the X-ray diffraction results of the powder specimen and bulk material can thus be ascribed to the deformation during the long period of iron ball milling. Even though the bulk samples present one phase structure, the powder diffraction patterns tend to be a mixture of seven-layered and tetragonal phases.

Two-dimensional scanning of X-ray scattering intensity with X'pert MRD can reveal extra reflections from the superlattice for single-variant martensite. By the phrase single variant it is meant that the sample contains only one short *c*-axis. The result is shown in Figure 5(a). The extra spots for the superlattice always appear in two directions, [110]* and $[1\bar{1}0]$*. This indicates that the modulation happens in two directions as well. Consequently, there should be present an interface separating these areas in which the modulation waves are nearly orthogonal to each other. The transmission electron microscopy image confirms this assumption. In Figure 5(b), the direction of the superlattice spots in the wide white band B is indeed orthogonal to the darker areas, marked A in the figure. The striations in the upper A area are the twin faults which are parallel with the shuffling plane. These striations cause corresponding steps in the upper interface. The lower interface is smoothly curved.

Figure 6, [P4], shows that the interface is seen as a saw-like boundary in medium magnification. Two sets of microtwins exist on both sides of the interface and their microtwin planes are orthogonal to each other. Apparently the microtwin planes are parallel to the (110) and $(1\bar{1}0)$ planes, respectively. The SAED taken at the interface area is identical to the addition two SAEDs taken from each side of the interface. Therefore, the crystal structure on both sides of the interface is identical if the superlattice is disregarded. The high-resolution image in Figure 6(b) reveals the interface structure on the atomic scale. It indicates that the interface consists of two constituent elements, which are referred to as "crossing" type and "step" type elements. In the step type element one set of the microtwins ends at the microtwin plane of the other domain and this forms one step with several microtwins. In the crossing configuration two domains have similar microtwin widths and the deformations of one domain are seen to penetrate to some extent into the other

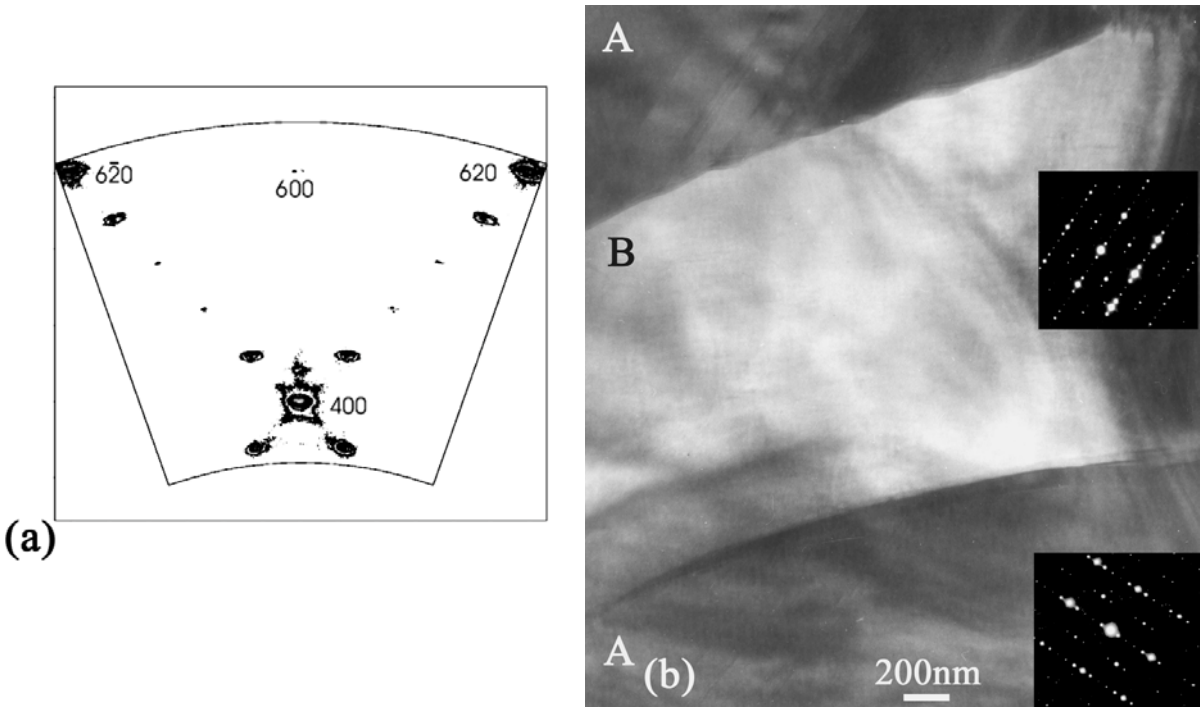

Figure 5. (a) The X-ray scattering intensity distribution shows additional spots in the conjugate [110]* directions obtained by using a two-dimensional scan and Epitaxy 3.0 software in the $Ni_{48.9}Mn_{30.8}Ga_{20.3}$ alloy. The diffraction is indexed with a tetragonal structure in the cubic coordinate system. (b) The bright field image of $Ni_{48.9}Mn_{30.8}Ga_{20.3}$ with corresponding SAED patterns from areas A and B, respectively [P4].

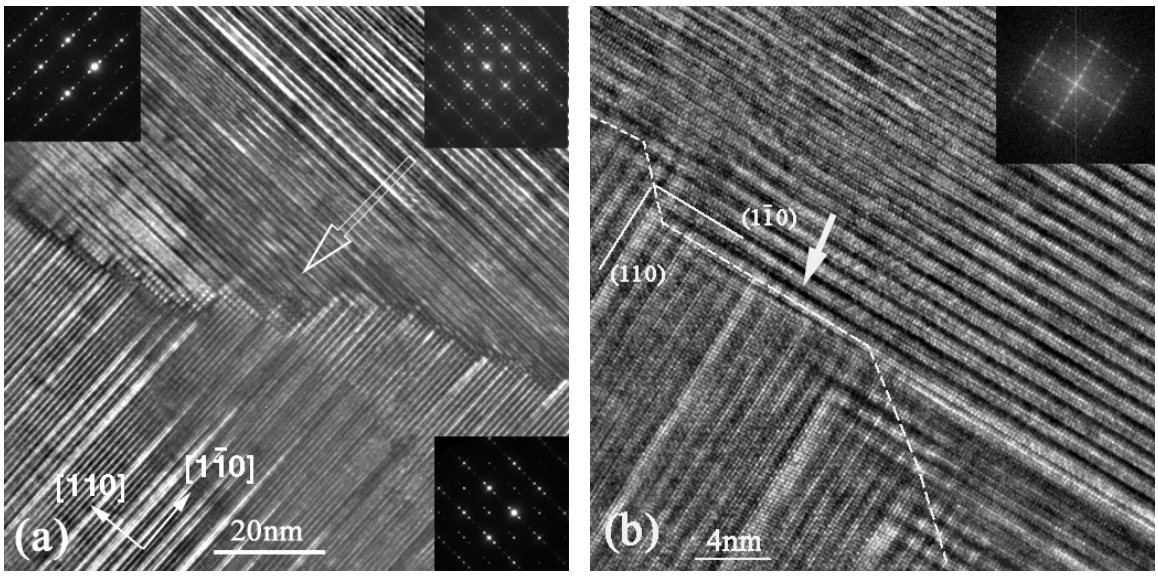

Figure 6. (a) The bright field image of the alloy $Ni_{49.5}Mn_{28.6}Ga_{21.9}$ alloy and the insets are the selected-area electron diffraction patterns from both sides of the interface and the interface area. (b) The atomic scale image of the interface, in the $Ni_{49.5}Mn_{28.6}Ga_{21.9}$ alloy and the insets are the FFT of the whole image [P4].

domain [67]. One step is indicated by the arrow in Figure 6(b), and the crossings come as transitions between steps. The Fast Fourier Transformation (FFT) of Figure 6(b) is identical to the selected area diffraction pattern made in the interface area.

The microtwin family can also be considered as twin faults, which is a basic structure for five-layered martensite. Thus, it is not surprising that there are, in addition, also other periodic twin faults other than the five in the sample. Figure 7, [P4], shows an example with several microtwin sets on the two sides of the interface having different periodicities. The top-left FFT shows a seven-layered superstructure and the low-left area a ten-layered superstructure. On the right, the top area is five-layered martensite. The lower-right FFT is obtained from the whole image, in which, on average, the left side consists of seven-layered martensite and the right side the five-layered one. The irregular twin faults are clearly visible in the whole area.

The angle between the two sets of the microtwin families is found to deviate slightly, within 1°, from 90°. This was measured in all the SAED patterns and FFTs for the two alloys that were studied. This angle corresponds to the angle between the (110) and $(1\bar{1}0)$ planes and it is also identical to the β angle in a big monoclinic unit cell. This suggests that the lattice parameter a is slightly different from b, which is in agreement with the X-ray powder diffraction refinement results.

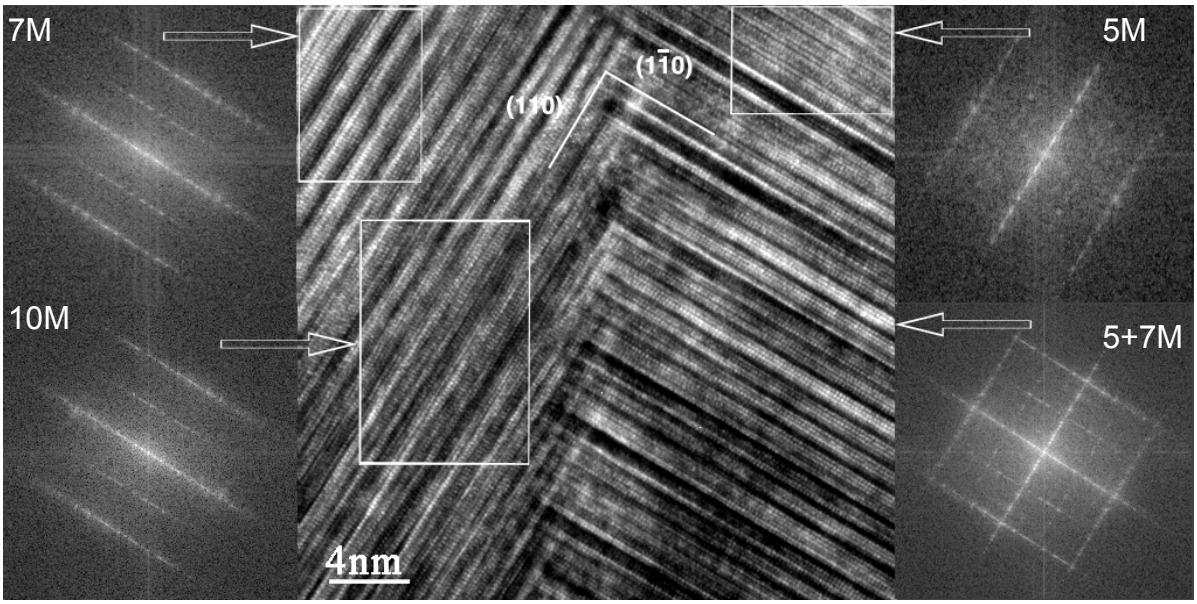

Figure 7. The interface and the irregular microtwin sequence on both sides of the interface. The microtwin sequence is determined from its FFT as seven-layered to ten-layered martensite from top to bottom on the left of the HRTEM image, five-layered, in the top on the right of the HRTEM image. The bottom FFT on the right of the HRTEM image is the FFT of the whole HRTEM image. The arrows indicate the area where the FFT is applied [P4].

3.3 Magnetic domains and their relationship with the twinning structure

The magnetic domain pattern was investigated by means of the Type I and Type II magnetic contrasts in SEM. The Type I magnetic contrast, also called the secondary electron contrast, arises from the secondary electrons emitted from the specimen and deflected by the stray field above the specimen surface [68,69]. To obtain this contrast the secondary electron detector is arranged asymmetrically and the specimen is oriented perpendicular to the incident electron beam. The magnetic signal for a given detector geometry depends on the integral over an electron trajectory. The integral is a smooth function over the stray field, even if the underlying domains have sharp boundaries. Therefore, Type I images are diffuse, mostly displaying the fundamental harmonic of the magnetic pattern. Because the Type I magnetic contrast is a pure trajectory contrast, the specimen must be oriented in such a way that the domains of one polarisation deflect the secondary electrons preferentially toward the detector, while those domains with the opposite polarity deflect the secondary electrons away from the detector. Figure 8, [P5], shows such an effect. Because the magnetisation vectors are nearly orthogonal to each other in the neighbouring twins, Figure 8(a) shows only one set of the domains in which the magnetisation vectors are parallel to the detector. After the specimen has been rotated 90°, another set of magnetic domains becomes visible in Figure 8(c).

Originally, the Type II magnetic contrast was described as the deflection of electrons on their path through the tilted specimen by the magnetic induction inside the specimen – either towards the surface, thus enhancing the backscattering yield, or away from the surface, with the opposite effect [68,69]. If the specimen is not tilted and the incident electron beam is normal to the sample surface, the magnetic field within the specimen can induce an angular asymmetry of backscattered electrons, which is detectable with a sectored backscattering detector [69,70]. Thus, the domain wall contrast is based on the accumulation of electrons scattered from both sides of the domain wall, as illustrated in Figure 9 [71]. Additionally, using the difference of the signal from the split detectors consisting of two semiannular parts, a clear domain contrast can be obtained.

Figure 8 shows the magnetic domain structures obtained from both the Type I and Type II magnetic contrasts. Even though the domain pattern in Figures 8(a) and 8(c) is blurred as a result of the mechanism of the Type I contrast, the results obtained with these two methods agree well with each other in Figures 8(a) and 8(b). The internal twins formed in the thermal martensite transformation are visible in all the big twin bands. However, in each big twin band there is one dominant internal twin variant, and the observed domain pattern is determined by the dominant variant. The viewed area was selected in such a way that the dominant variant in each band has its *c*-axis in plane. Each band consists of many plate-like or dagger-shaped 180° magnetic domains, as shown in Figure 8(d). The trace of the minority twin variant shows a zigzag pattern. This phenomenon was also studied with the optical microscopy. It was confirmed that the surface is tilted in the opposite direction along the opposite magnetisation vector polarity. Consequently, the zigzag pattern of the minority twin variant is caused by the tilted surface.

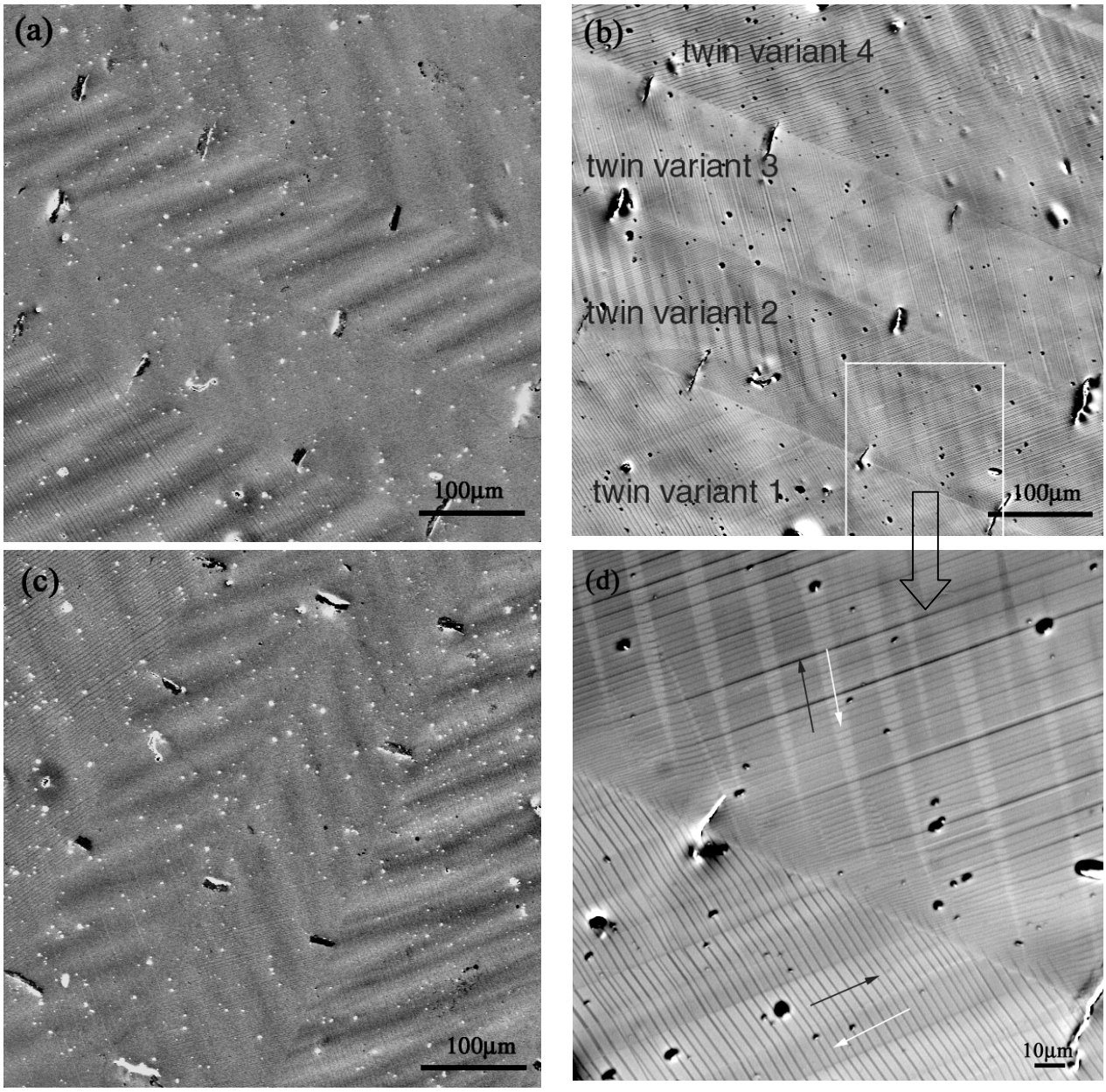

Figure 8. The magnetic domain structure in the multi-variant state of the $Ni_{48.9}Mn_{30.8}Ga_{20.3}$ alloy: (a) with Type I magnetic contrast; (b) with Type II magnetic contrast; (c) the same area as in (a) after 90° rotation with Type I magnetic contrast; (d) the enlarged view from the rectangular area in (b) with Type II magnetic contrast (The magnetisation vector is indicated by arrows) [P5].

The Type II magnetic contrast images were collected with the composition (COMPO) mode by summing all the signals from four quadrant backscattering detectors. It is clear from the previous discussion that only the domain wall contrast is visible with the COMPO mode. However, the domain contrast is also visible in our observation. It is assumed that the domain contrast arises from the asymmetry of the collection efficiency of backscattered electrons from opposite magnetisation. There are many factors that could cause this, such as the different domain width, the fact that the incident beam is inclined to the sample surface, and the arrangement of the geometry between the magnetisation vector, electron beam, and four quadrant detectors. It is also assumed that the contrast contribution from the surface relief can be ignored in the COMPO image. The surface relief

can either enhance or suppress the magnetic contrast because it influences the collection efficiency of the backscattered electrons by changing their emission path. Thus the grey level of the digital image inside one domain will be uneven. However in our observation the grey level of the image inside one domain is quite even and it is quite realistic to consider that the COMPO mode image shows only the contribution of the magnetic contrast. Figure 10, [P5], demonstrates the magnetic domain contrast together with the magnetic domain wall contrast with a backscattered electron image (BEI). The specimen is in a two-variant state obtained by means of the controlled magnetisation process. The internal twin variants inside the big twin band have mostly disappeared. This pattern is typical of the two-variant state in which the *c*-axis in each variant is in plane. The magnetic domains follow the easy axis of the each variant, creating a staircase-like pattern. The 90° domain wall coincides with the twin boundary. Both the 90° and 180° domain wall contrasts are visible as black and white lines between domains.

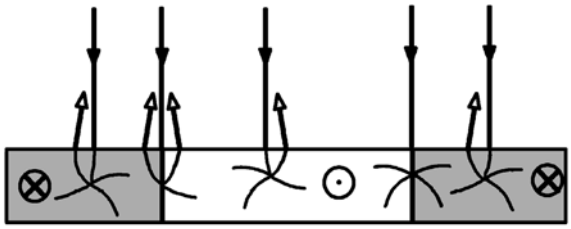

Figure 9. The magnetic domain contrast and the domain wall contrast formation in the SEM at normal incidence with a sectored backscattering detector under an objective lens [71].

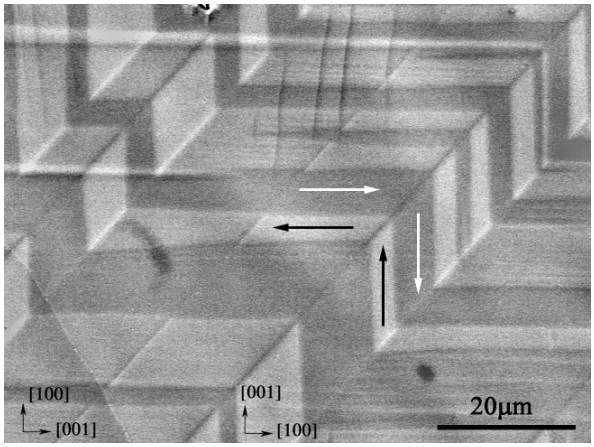

Figure 10. The two-variant specimen with the 180° magnetic domain pattern coupled with the twin band (BEI) [P5].

Figure 11, [P5], demonstrates the dramatic change of the magnetic contrast in the COMPO and topography (TOPO) modes, respectively. A TOPO mode image is created by turning off two diagonal quadrants and using the difference signal from the two remaining diagonal quadrants. The magnetic domain contrast will be clearly visible in this mode, according to Figure 9. Figure 11(a) is a COMPO mode image, and, following the foregoing discussion, it can be considered as a pure magnetic contrast. Figure 11(b) is a TOPO mode image. First, all the domain wall contrast disappears. The 180° domain contrast is considerably enhanced. The 90° domain contrast is

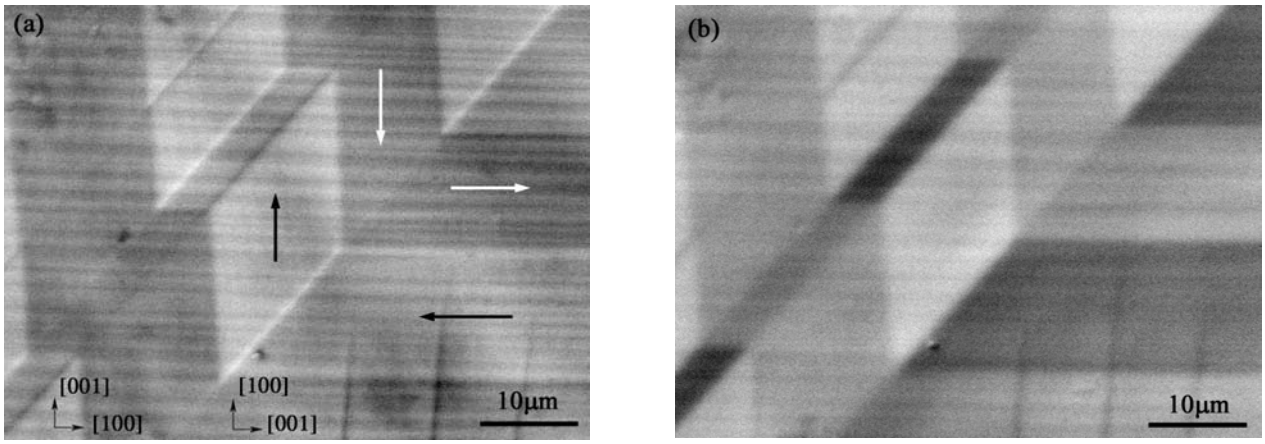

Figure 11. The Type II magnetic contrast of a two-variant specimen; (a) in the COMPO mode, and (b) in the TOPO mode [P5].

dramatically enhanced in the direction of one magnetisation vector. It is unclear why this enhancement happens in only one magnetisation direction. It is possibly related to the geometrical relationship between the magnetisation vector and the two quadrants of the backscattering detector. Thus, in the TOPO mode the contrast is a combination of both the magnetic and topographic contrasts.

The internal twins disappear from most of the area of the specimen after the controlled magnetisation, when the two-variant state forms. However, in some areas the internal twins remain. One such area is shown in Figure 12, [P5]. Here the (101) twin boundary consists of a thin layer (indicated by the white dashed lines) instead of a line as in Figure 11(a). The end tips of the traces of the internal twin cross each other at some places along the boundary (Figure 12). On the right side of the twin boundary there are regular 180° domains, i.e., parallel plate-like domains, while on the left side the 180° domains are more dagger-like. On both sides of the boundary the minority twin variant traces show a zigzag pattern. The possible reason and the orientation relationships of the structures in this image will be discussed in the next section.

Next, this specimen is further magnetised to one variant. The new domain structure is shown in Figures 13(a) and 13(b) by means of Type II and Type I magnetic contrasts, respectively. The Type

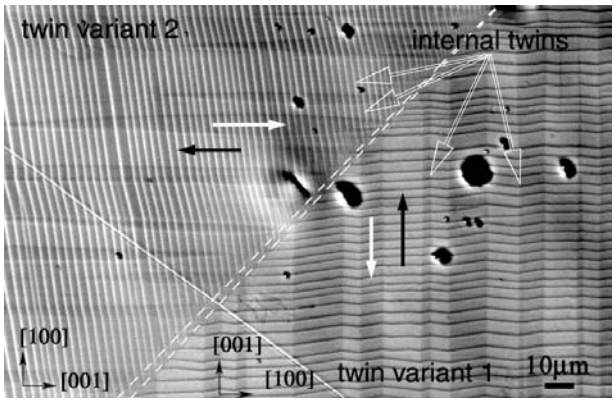

Figure 12. The (101) twin boundary and the remaining internal twins (BEI) in the two-variant specimen [P5].

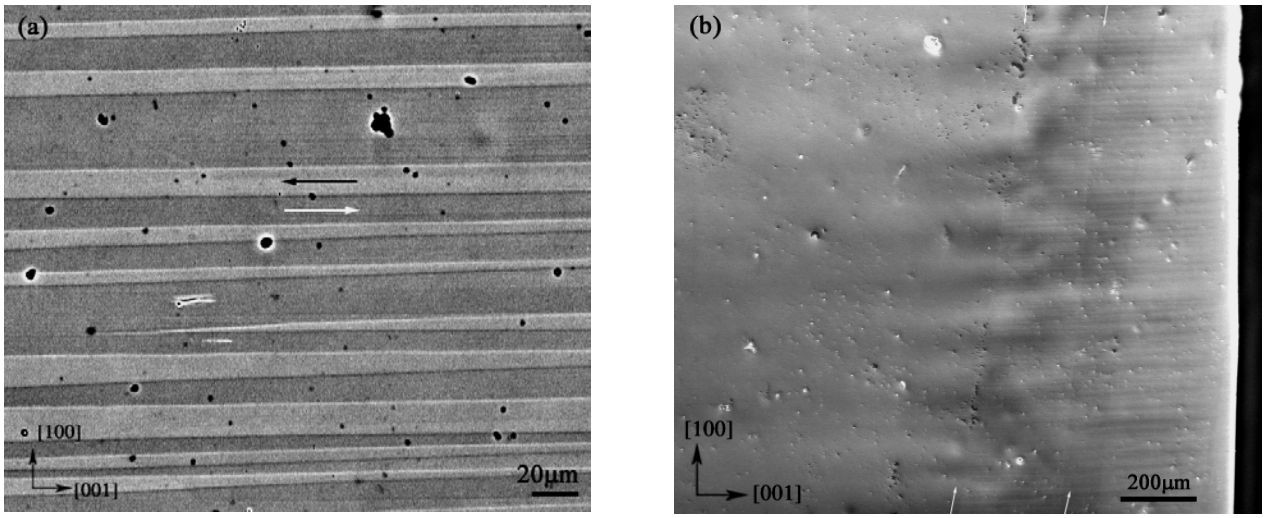

Figure 13. The single-variant specimen with the 180° domains is imaged by (a) Type II contrast and (b) Type I contrast. [P5]

II contrast reveals that the 180° domains run through the observed surface. In Figure 13(b) the Type I contrast image, which is created at very low magnification, shows the 180° domain branching into fine domains at the edge of the specimen. The observed domain width varies in the range of 1 – 30 μm.

When speculating on the possible mechanism for the above mentioned zigzag pattern of the minor variant, it was clear that the morphology should be studied by means of optical microscopy. It turned out that the structure of magnetic domains was clearly visible, together with this zigzag pattern. This indicates that the magnetic domain structure is associated with a large surface relief. Figure 14 shows one such zigzag pattern observed by means of optical and scanning electron microscopy [P6]. This discovery provides a new method for studying the relationship between the twinning structure and the magnetic domain pattern.

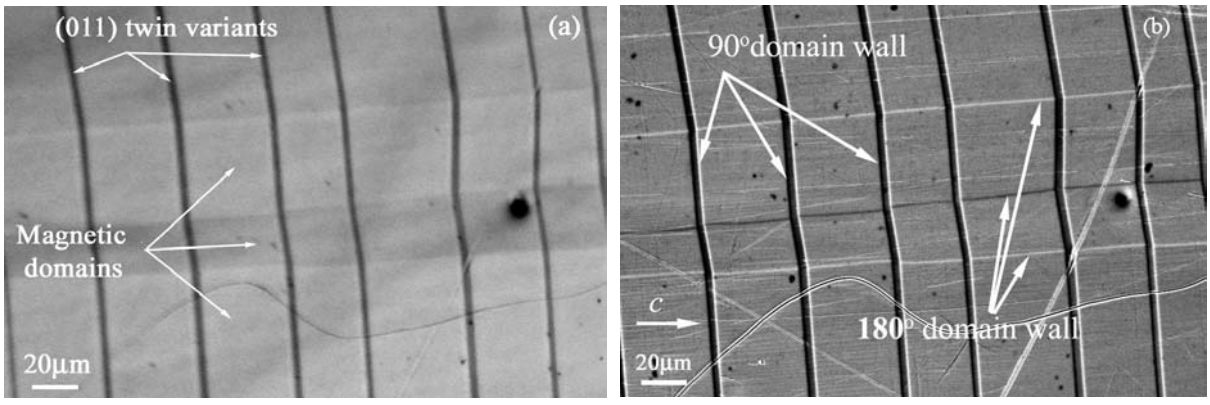

Figure 14. (a) Optical image of 180° domains (broad horizontal band) and (011) twins (dark vertical line); (b) BEI shows the same area as in (a), and the domain wall contrast is visible as alternating white and dark lines. The *c*-axis of the dominant variant is horizontal and the *c*-axis in these dark vertical lines is perpendicular to the observed surface [P6].

Thereafter, the study of the evolution of the magnetic domain structure in the applied magnetic field was carried out on the $Ni_{49.5}Mn_{28.6}Ga_{21.9}$ alloy by means of an optical microscope. At the beginning of the study, the specimen contained macroscopically one single martensite variant. Then it was magnetised to another single-variant state. The optical image was taken every time the applied field was removed. In Figures 15(a), (b), and (c), the preceding field was applied horizontally, while its direction was vertical before Figures 15(d), (e) and (f). The field was applied again horizontally before Figures 15(g), (h) and (f). The observed surface is the (010) plane and the applied field exchanges the *a*- and *c*-axes. However, there exist a small number of other variants, too. These minority variants are categorised according to their twin boundary with the dominant variant. Figures 15(b) and (c) show the enlarged view of the upper-left area and the lower-right area of Figure 15(a), respectively. In the same way, Figures 15(e) and (f) and Figures 15(h) and (i) are enlarged views of Figures 15(d) and 15(g), respectively.

In Figure 15(a), the visible domain structure shows 180° domains that run horizontally on the observed surface, which agrees with the direction of the preceding applied field. Figure 15(b) shows the coupling of the domain structure with the (101) twin variants to form a staircase-like domain pattern, as in Figure 10. Figure 15(c) shows the 180° domain intersection with the (011) twin variants. It is noted that in the image the grey levels of the (101) twin variants are only slightly different from that of the majority variant, but the (011) twin variants are visible as vertical black lines. The formation of the (101) twins is not accompanied by the surface relief on the (010) plane, while the (011) twins cause surface relief on the (010) plane. Thus, the weak contrast of the (101) twin variants arises from their crystallographic orientation, and the deformation of the dark lines of the (011) twin variants is caused by the tilted surface. The (011) twin variants show a zigzag pattern similar to that in the SEM image. Another feature noticed in Figure 15(c) is the weakly visible grey vertical plate, which, we postulate, results from the surface relief of the magnetic domain before polishing [P7].

In Figures 15(d), (e), and (f), taken after a magnetic field of 1 T was applied vertically, the previous magnetic domain structure and twin variants totally disappear. New 180° domains are formed vertically. There are only traces of the (101) twin variants visible in the observed area. Additionally, the crack grows further. Figure 15(c) shows that the newly formed 180° domains tend to occupy the residual surface relief as these deformations are types of imperfections on the surface.

Figures 15(g), (h), and (i) show the change in the structure after a magnetic field of 1 T was applied horizontally. Now, the crystallographic structure becomes complicated. A (101) twin band approximately 70 μm wide forms with a substructure inside. The (011) twin variants are wider than the ones in Figure 15(a). The domain structure becomes irregular. The 180° domains in the upper area still follow the preceding field direction. However, in the rest of the image it is hard to detect any visible domain structure, though there are some fine lines with very weak contrast in the middle of Figure 15(i). The residual surface relief is still visible as weak grey strips, since they can only be removed by polishing.

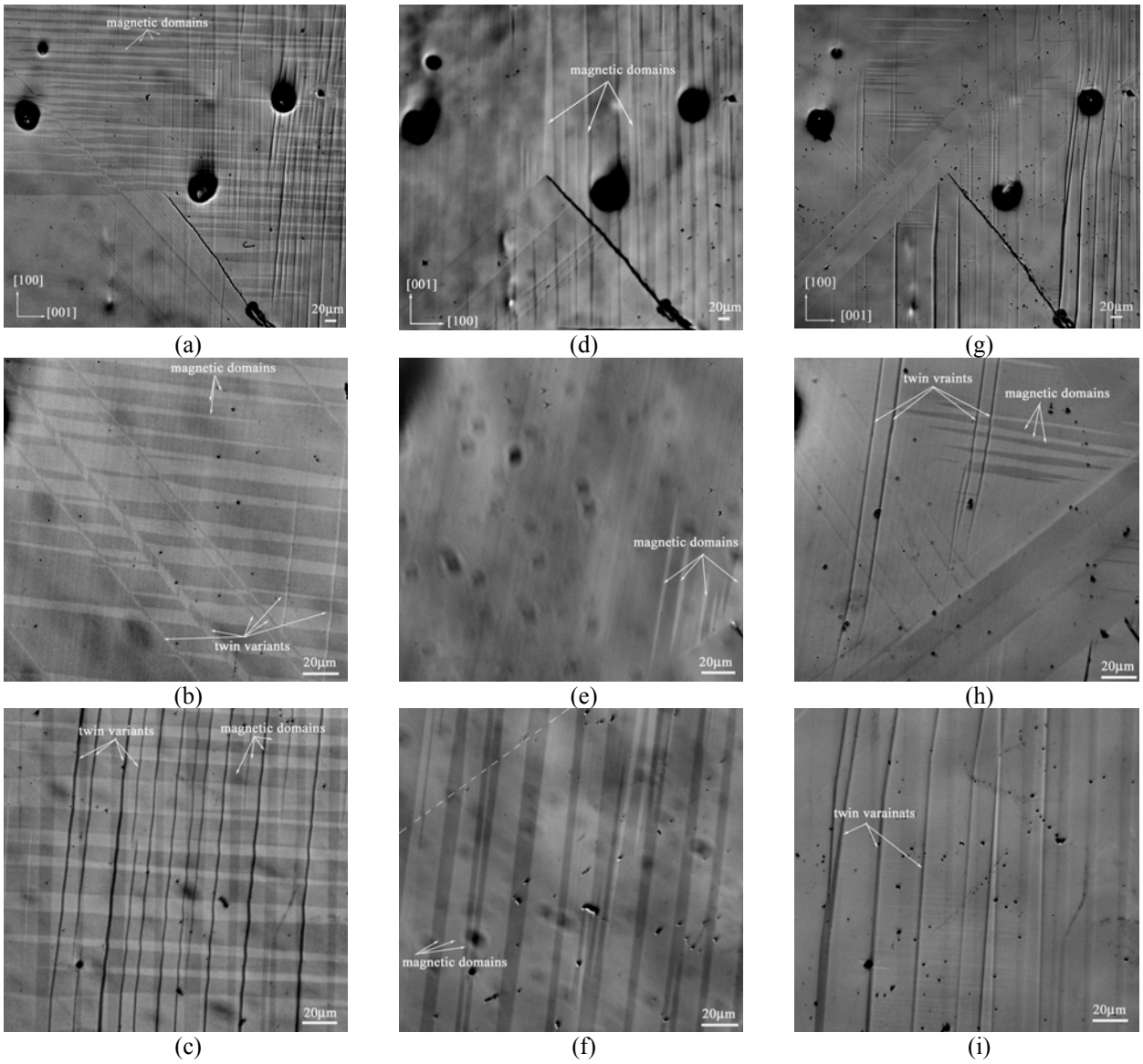

Figure 15. The evolution of the magnetic domain structure that is in-plane with the specimen surface during the changing of the direction of the magnetic field, viewed by means of optical microscopy. Prior to polishing, a magnetic field of 1 T was applied to the short dimension of the surface being observed (i.e., vertically in the images). Then, after polishing, the field of 1 T was applied along the long dimension of the surface (horizontally). The resulting images are shown on the left; (a), (b), and (c). In the images in the middle, (d), (e), and (f), the previous field was applied along the short dimension of the surface (vertically), and in the images on the right, (g), (h), and (i), again horizontally. The images in the second and third rows are magnifications of the upper-left and bottom-right areas of the images in the first row, respectively [P7].

Figure 16 shows a detail of the same area as in Figure 15(i) using BEI. In the optical image the magnetic domain structure is not visible. The BEI reveals the existence of fine horizontal magnetic domains. The whole area consists of very fine domains with a typical width of 2 µm.

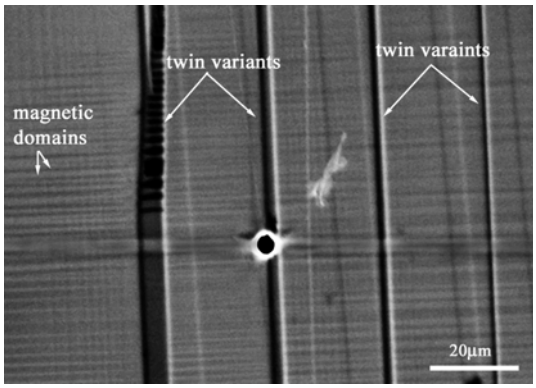

Figure 16. BEI utilising Type II magnetic contrast reveals the fine magnetic domains that are nearly invisible in the optical image Figure 15(i) [P7].

Another area in which no domain structure was visible in the optical image was also investigated with the SEM backscattered electron image, shown in Figures 17 (a) and (b). The optical image in Figure 17(a) shows a firtree-like domain pattern near the (101) twin boundary, while the BEI in Figure 17(b) suggests that the firtree-like domain is part of a larger 180° domain structure. This confirms that the surface relief observed optically is really due to the magnetic contrast. Figures 16 and 17 also suggest that if there is no contrast in the optical image, the magnetic domains are either not accompanied by the surface relief or the region consists of very fine domains.

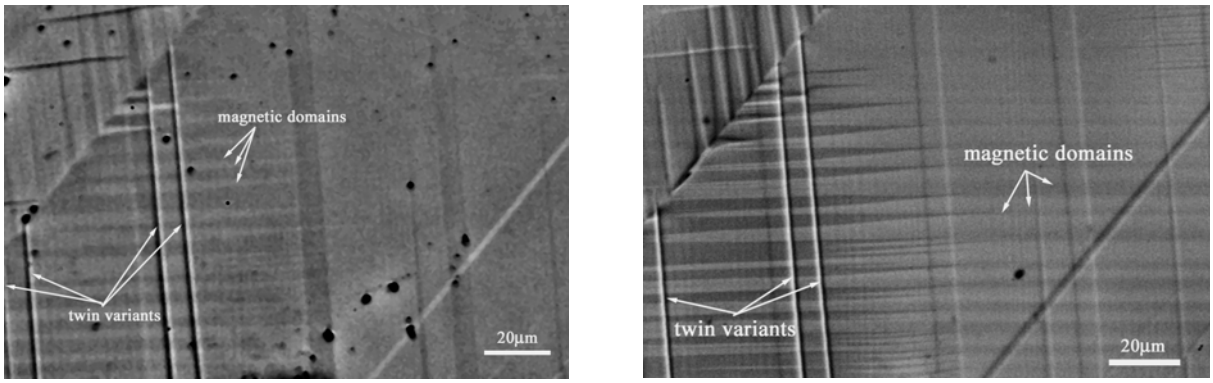

(a) (b)

Figure 17. (a) An optical image with a firtree-like magnetic structure close to the twin boundary; (b) The BEI of the same area, again revealing the firtree-like structure extended with the 180° domain by utilising Type II magnetic contrast. This demonstrates that the observed non-homogenous surface relief in the optical image is connected to the magnetic contrast [P7].

4. DISCUSSION

4.1 Twinning system in a Ni-Mn-Ga alloy.

Both the X-ray and electron diffraction investigations suggest that the basic structure of the Ni-Mn-Ga alloy that was studied deviate slightly from a tetragonal one in five-layered martensite. The tetragonal structure may still be used as a simplified mode for the analysis of the twin system in five-layered martensite. Thermally formed martensite is internally twinned after the phase transformation. These internal twins are on micrometer scale, so they can be detected by the optical microscopy. This should be ascribed to the small transformation strain, which can be expressed as:

$$\begin{bmatrix} \eta_1 & 0 & 0 \\ 0 & \eta_1 & 0 \\ 0 & 0 & \eta_3 \end{bmatrix} = \begin{bmatrix} 1.019 & 0 & 0 \\ 0 & 1.019 & 0 \\ 0 & 0 & 0.961 \end{bmatrix}, \qquad (4\text{-}1)$$

where η_1 and η_3 are the deformation parameters, $\eta_1 = a_t/a_c$ and $\eta_3 = c_t/a_c$, which are calculated from the lattice parameters of the $Ni_{49.5}Mn_{28.6}Ga_{21.9}$ alloy. The measured lattice constants of the parent and martensitic phases are a_c = 5.837 Å, a_t = 5.95 Å and c_t = 5.61 Å [P3].

The cubic-to-tetragonal transition has been widely analysed with the methods of the geometrically nonlinear theory of martensitic transformation [72,73,74]. The solutions suggest that martensite is a twinned microstructure determined by the crystal lattice parameters. All the twin pairs are compound twins. The twin plane is the $\{110\}_c$ plane, which becomes the {101} plane of the tetragonal lattice. The internal twins are twinned in the same plane. We can analyse the internal twins in Figure 12. The specimen is oriented according to the cubic axis, and thus the twin boundary is (101). The observed surface is (010), and the possible internal twin plane may be either the $(10\bar{1})$ plane or a {011} type plane. The trace of the {011} planes on the (010) plane is parallel with the *a*-axis. Thus, the trace of the $(10\bar{1})$ plane on the (010) plane will form an angle of 93.75° with the (101) twin plane and the trace of the {011} will form an angle of 43.22° with the (101) twin plane. The angle between the internal twin boundary and the (101) twin boundary on the both sides of the (101) plane can be measured from Figure 12. The angle on the right side of the (101) twin boundary is approximately 45° and on the left side 52°. This suggests that on the left side the surface is more close to the (010) plane and this is the reason why the magnetic domains are straight parallel bands. On the left side, the surface deviates by nearly 9° from the (010) plane. Now the magnetic domain structure is dagger-like, so as to avoid the free-pole on the surface. Additionally, the (101) twin boundary in Figure 12 is not a planar boundary, but more like a thin layer. During the martensitic transformation, the transformation front is an accommodation layer for the subsequent martensitic twins. This accommodation region consists of extremely fine twins which can accommodate the transformation strain. The width of the layer varies with the local temperature gradient, the velocity of the transformation, and the local residual stress. If the transformation strain is relatively small, the accommodation layer will be quite narrow, as can be seen from Figure 8, and thus the twin boundary is nearly planar. As a results of the local conditions during the transformation the accommodation region has become wider in Figure 12. This may be the reason why the internal twins near this twin boundary do not disappear during the controlled magnetisation process.

The HRTEM image shows that each martensite variant consists of stacking twins with their twin plane along the {110} plane. This is because each martensitic variant contains two modulation waves propagating along the (110) and $(1\bar{1}0)$ planes, respectively. These stacking twins, or microtwins, are usually several nanometers thick. The boundary between these two families of microtwins consists of both step and crossing elements. Therefore, this boundary is a curved interface and parallel to the *c*-axis. The schematic view of the martensitic morphology that is a combination of these macroscopic and microscopic twins is shown in Figure 18. The orientation of the {101} planes and (110) plane is shown in Figure 18(b).

The volume fraction of the twin variants was estimated from Figure 19 in the following way. The areas to be analysed were selected from both sides of the (101) twin boundary in Figure 12. The images were transferred into a black-and-white mode. Then the ratio of the black pixels to the white pixels was analysed using the free UTHSCSA ImageTool program (developed at the University of Texas Health Science Center at San Antonio, Texas and available from the internet by anonymous FTP from ftp://maxrad6.uthscsa.edu). The results are shown in Figure 19. According to the nonlinear geometry theory, the volume fraction, λ, can be calculated [72]:

$$\lambda = \frac{1}{2}\left(1 - \sqrt{\frac{2\left(\eta_3^2 - 1\right)\left(\eta_1^2 - 1\right)\left(\eta_1^2 + \eta_3^2\right)}{\left(\eta_3^2 - \eta_1^2\right)} + 1}\right). \qquad (4\text{-}2)$$

The calculated numerical value of λ is 0.32. This is close to the measured value of the fraction of the black pixels, 0.325, in Figure 19(a). However, in Figure 19(b) the fraction of the black pixels, 0.246, is much less than the calculated value of the volume fraction of the twin variant, 0.32. However the above equation is valid only at the transformation temperature and the distribution of the variants may be localised at lower temperatures [76].

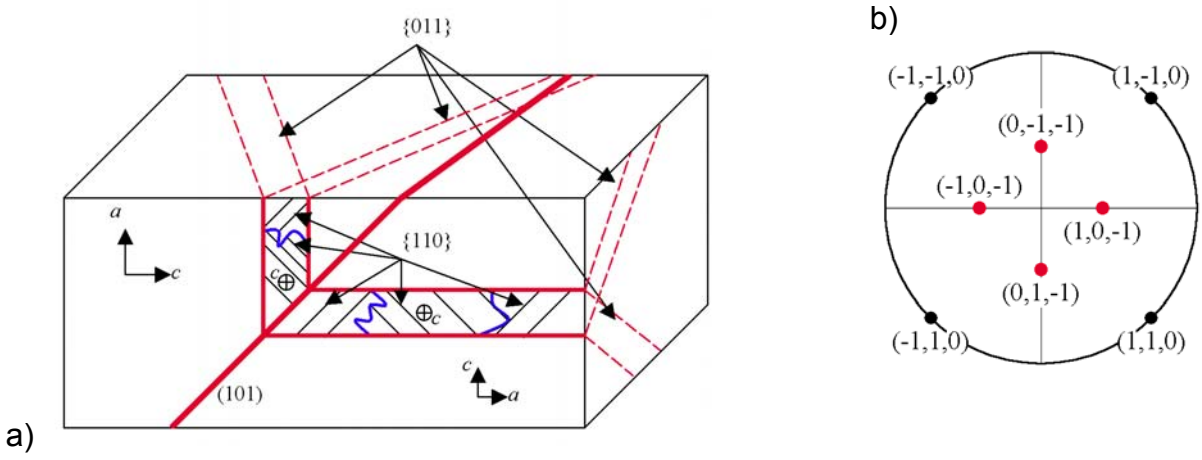

Figure 18. A schematic view of the Ni-Mn-Ga hierarchical twinning structure. a) The microtwins are indicated only in two internal twins with their *c*-axes perpendicular to the front surface. The dashed lines on the right and on the top surface are the traces of the {011} plane. There are two possibilities for this trace in each case and, therefore, there are two sets of dashed lines. b) The pole figure shows the orientation relationship of {101} planes and (110) plane.

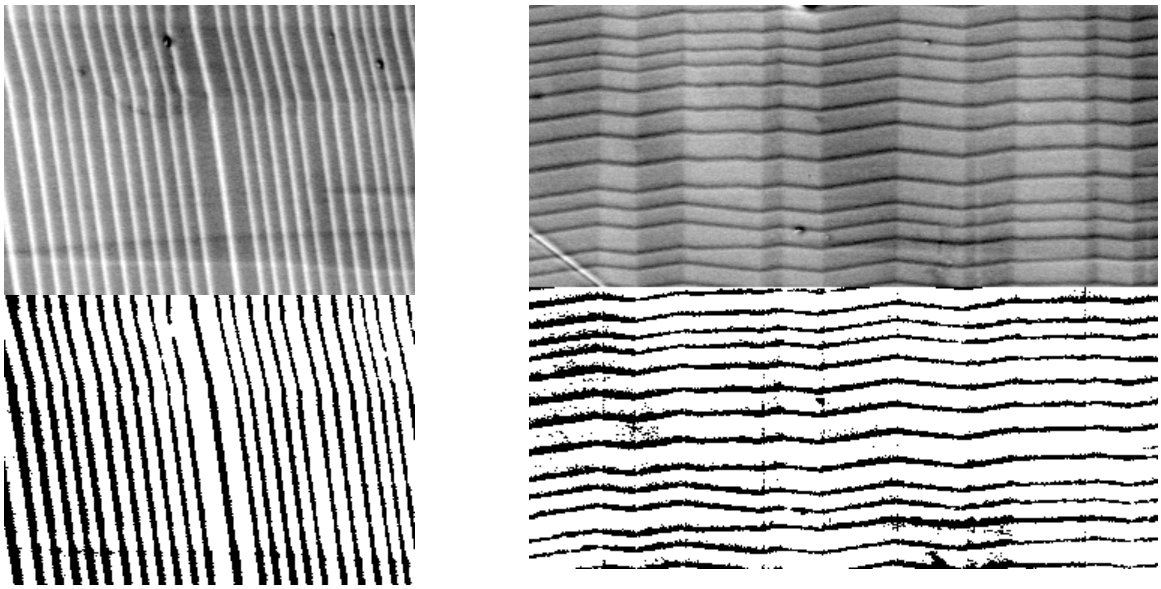

(a) Fraction of the black pixels is 32.5% (b) Fraction of the black pixels is 24.6%

Figure 19. Two areas selected from the both sides of the twin boundary in Figure 12 are used for analysing the volume fractions of the twin variants.

4.2 The magnetic domain structure and its surface relief

The direct optical magnetic domain observation has previously been reported for a Terfenol-D crystal, where the magnetostriction effect causes surface tilting [75]. In our case, with a Ni-Mn-Ga alloy, the optical magnetic contrast appears as a result of the surface undulation and its origin is different from that of Terfenol-D.

When the saturation magnetic field is applied, the specimen with the five-layered martensite structure adopts a nearly single-twin-variant state and contracts by 6% in the magnetisation direction. However, some residual twin variants with a different orientation can remain in the structure as the MSM effect does not take place in them. These residual variants cause straining of the specimen. Furthermore, the inclusions, point defects or other imperfections of the lattice may alsocause straining. The residual variants have their easy magnetisation axis, i.e. their short crystallographic axis (*c*-axis), roughly perpendicular to the *c*-axis of the surrounding major twin variant. Therefore, they behave in a magnetic field in a differently way from the major part of the structure, which can generate additional strain, resulting in compressive stress. After the removal of the magnetic field, the magnetic vector of the residual variants rotates back towards their easy axis and the previous compressive stress is gradually reduced by the reverse movement of the twin boundaries. Consequently, reverse elongation in the direction of the previous magnetisation takes place – strains of 0.3% [77] and 0.41% [78] have been observed. Because of the volume conservation, this elongation in one direction will result in contraction in perpendicular directions.

In the saturation magnetic field the whole sample is a single magnetic domain. When the field is reduced, the single domain breaks down into a multi-domain structure by the demagnetisation field. These new magnetic domains start to nucleate at the surface. The free surface may undergo less contraction than the bulk material under it. This produces the roofed or corrugated shape of the

surface illustrated in Figure 19(a). Simultaneously, the surface undulation may assist the nucleation of the domain walls. In the end, the magnetic domain walls are pinned at the ridges and the valleys of the surface. On the other hand, it may also be that the newly nucleated domain walls serve as formation sites for the surface corrugation, i.e. for the ridges and valleys. Consequently, the surface relief connected to the magnetic domains is caused by the reduction of the internal energy by the magnetic interactions and the accommodation of the internal strains between the differently oriented twins. This mechanism seems to be quite non-homogeneous and random and, thus it may lead to different metastable configurations during successive magnetisations.

The ridges and valleys, which coincide with the domain walls, follow these domain walls across the (101) twin boundary, without a change in height between the ridge and the valley. Thus the (101) twin boundary stays straight, even though the roofed surface morphology follows the direction of the new magnetisation (and crystallographic), which is nearly perpendicular to the previous direction. This creates the staircase pattern observed in [P5,50]. Consequently, this surface undulation is totally compatible when domains cross the (101) twin boundary.

The trace of the (011) twin is a different case. When the surface undulations meet at the (011) twin boundary, the trace of this twin boundary turns from the straight line by the lifted surface. Since the martensite lattice parameters for the alloy under study are a = 5.95 Å and c = 5.61 Å, the (011) twin boundary intersects with the (010) surface at 46.7°. As the twin trace crosses the ascending and descending parts of the corrugated surface, the (011) twin trace forms a zigzag pattern on the projection surface, i.e., on the (010) plane. The angle derived from the zigzag shape of the (011) twin boundary can be used to calculate the extent of surface undulation.

Let θ be the intersection angle between the (011) and (010) planes in martensite, i.e., θ = 46.7° for the alloy under study. α is the angle between the projection of the (011) twin trace on the (010) plane and the [100] direction, while β is the angle of the tilted surface; see Figure 20(a). Then, by the geometrical relationship, the angle β is given by

$$\tan\beta = \tan\alpha\tan\theta. \qquad (4\text{-}3)$$

Here, α can be obtained from the figure as half of the angle between two adjacent lines of the zigzag twin boundary trace. The average angle measured from Figure 15(c) is 1.85° and, therefore, the calculated tilt angle β is 1.96°.

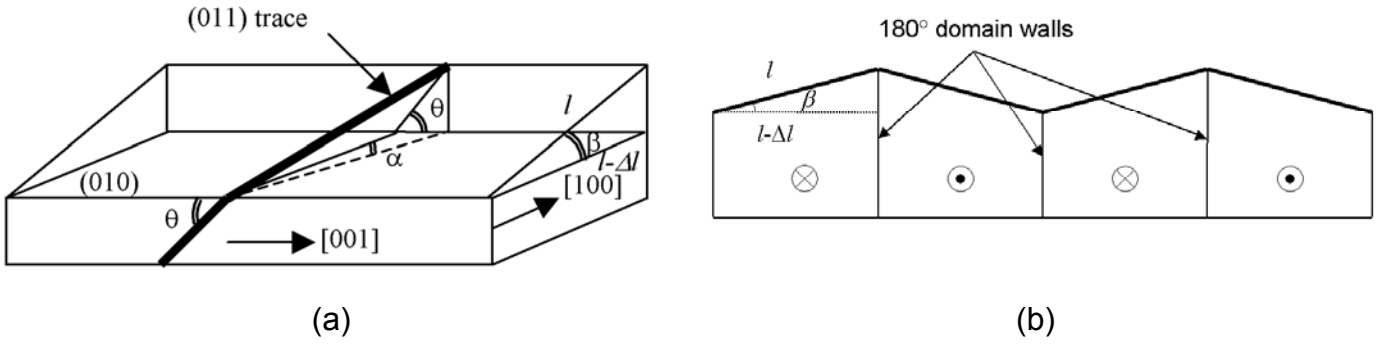

(a) (b)

Figure 20. (a) An illustration of the surface relief and the magnetic domain configuration; (b) a model of the projection of the (011) twin configuration on the tilted surface.

The contraction strain needed for the observed tilting can be calculated with the β angle from the relationship:

$$\frac{\Delta l}{l} = 1 - \cos\beta \quad , \qquad (4\text{-}4)$$

where l is the original length on the surface, and Δl is the contraction of the bulk material under the surface, as depicted in Figure 20(b). The average strain that causes the observed tilting of the surface is 0.059%, corresponding to an elongation of 0.11% in the direction of magnetisation. This is comparable with the previously reported reversible strain of 0.41%. Furthermore, the compressive stress may not be completely released by the surface relief.

5. CONCLUSIONS

The crystal structure, twin boundary microstructure, and magnetic domain pattern together with the twinning structure were studied in this thesis work. On the basis of the results presented, the following main conclusions can be drawn:

- The chemical composition of Ni-Mn-Ga alloys can be determined reliably by WDS and EDS-analysis, applying an excitation voltage of 20–30 kV and the K_α line for the Ga element.

- The crystal structure of five-layered martensite determined by X-ray powder diffraction is consistent with that obtained by single crystal X-ray diffraction. Five-layered martensite can be well described as a modulation structure.

- The basic structure derived from the X-ray powder diffraction measurement is a monoclinic lattice. This is confirmed further by HRTEM study, which shows that the length of the *a*-axis is slightly different from that of the *b*-axis. The stacking order model cannot take into account the non-uniform transformation shear. The HRTEM image showed that the modulation wave propagates in two directions, (110) and $(1\bar{1}0)$, respectively.

- On a macro-scale, the thermally formed martensite consists of the twin bands with an internal twin structure. The internal twin plane is {101} planes. On a nano-scale, five-layered martensite has a microtwin feature with two sets of microtwin planes corresponding to two modulation wave vectors of the (110) and $(1\bar{1}0)$ planes. The interface between these two sets of microtwins, i.e. the macrotwin boundary, is hinted at by X-ray diffraction and disclosed in the HRTEM image. The macrotwin boundary consists of two constituent elements of step and crossing types.

- The magnetic domain structure is visualised by Type I and Type II magnetic contrasts in SEM. In five-layered martensite, the magnetisation vectors are parallel and anti-parallel to the *c*-axis separated by a 180° domain wall within one variant. When crossing a twin boundary, magnetisation vectors continue to follow the *c*-axis in the adjacent variant. Thus the 90° domain wall is coincident with the {101} twin boundary.

- The direct observation of the magnetic domains indicates a large magnetic domain associated surface relief. This surface relief causes the (011) twin variant traces to be zigzag-patterned, when projected on the (010)-plane. The surface relief is believed to arise from the different straining of the surface and the bulk material. The straining calculated from the present model is comparable with experimental values.

- The direct optical observation of the evolution of magnetic domain patterns, by applying a magnetic field in two perpendicular directions alternately, shows that the magnetic domain pattern and configuration of the twins take a unique path even though the magnetic field-induced strain is reproducible.

REFERENCE LIST

[1] Ullakko, K., Huang, J. K., Kantner, C., O'Handley, R. C. and Kokorin, V. V. Large magnetic-field-induced strains in Ni_2MnGa single crystals. *Applied Physics Letters,* **69,** (1996), 1966-1968.

[2] Hames, F. A. Ferromagnetic-alloy phases near the compositions Ni_2MnIn, Ni_2MnGa, Co_2MnGa, Pd_2MnSb, and PdMnSb. *Journal of Applied Physics,* **31,** (1960), 370S-371S.

[3] Webster, P. J. Heusler Alloys. *Contemporary Physics,* **10,** (1969), 559-577.

[4] Webster, P. J., Ziebeck, K. R. A., Town, S. L. and Peak, M. S. Magnetic order and phase transformation in Ni_2MnGa alloy. *Philosophical Magazine B: Physics of Condensed Matter: Statistical Mechanics, Electronic, Optical and Magnetic Properties,* **49,** (1984), 295-310.

[5] Kanomata, T., Shirakawa, K. and Kaneko, T. Effect of hydrostatic pressure on the Curie temperature of the Heusler alloys nickel-manganese-Z (Ni_2MnZ) (Z = aluminum, gallium, indium, tin and antimony). *Journal of Magnetism and Magnetic Materials,* **65,** (1987), 76-82.

[6] Fujii S., Ishida S. and Asano S. Electronic structure and lattice transformation in nickel-manganese-gallium (Ni_2MnGa) and cobalt-niobium-tin (Co_2NbSn). *Journal of the Physical Society of Japan,* **58,** (1989), 3657-65.

[7] Kokorin V. V. and Chernenko V. A. Martensitic transformation in ferromagnetic Heusler alloy. *Physics of Metals and Metallography,* **68,** (1989),111-115.

[8] Zasimchuk I. K., Kokorin V. V., Martynov V. V., Tkachenko A. V. and Chernenko V. A. Crystal structure of martensite in Heusler alloy Ni_2MnGa. *Physics of Metals and Metallography (translation of Fizika Metallov i Metallovedenie),* **69,** (1990), 104-108.

[9] Kokorin V. V., Martynov V. V. and Chernenko V. A. Stress-induced martensitic transformations in nickel manganese gallium (Ni_2MnGa). *Scripta Metallurgica et Materialia,* **26,** (1992), 175-7.

[10] Martynov V. V. and Kokorin V. V. The crystal structure of thermally- and stress-induced martensites in nickel-manganese-gallium (Ni_2MnGa) single crystals. *Journal de Physique III,* **2,** (1992), 739-49.

[11] Martynov V. V. X-ray diffraction study of thermally and stress-induced phase transformations in single crystalline Ni-Mn-Ga alloys. *Journal de Physique IV,* **5,** (1995), 91-99.

[12] Overholser R. W., Wuttig M. and Neumann D. A. Chemical ordering in Ni-Mn-Ga Heusler alloys. *Scripta Materialia,* **40,** (1999), 1095-1102.

[13] Nishiyama Z. *Martensitic transformation,* Academic Press (1978), 74-108.

[14] Noda Y., Shapiro S. M., Shirane G., Yamada Y. and Tanner L. E. Martensitic transformation of a nickel-aluminum alloy. I. Experimental results and approximate structure of the seven-layered phase. *Physical Review B: Condensed Matter and Materials Physics,* **42,** (1990), 10397-10404.

[15] Murakami Y., Otsuka K., Hanada S. and Watanabe S. Self-accommodation and morphology of 14M (7R) martensites in an Ni-37.0at.%Al alloy. *Materials Science and Engineering A*, Vol. **A189**, (1994), 191-199.

[16] Otsuka. K, Ohba. T, Tokonami. M, and Wanyman C.M, New description of long period stacking order structures of martensites in β-phase alloys, *Scripta Metallurgica et Materialia* **29** (1993), 1359-1364.

[17] Inoue T., Morito S., Murakami Y., Oda K. and Otsuka K. New martensite structures and composition dependence of martensitic transformations in $Ni_{50}Al_xMn_{50-x}$ alloys. *Materials Letters,* **19,** (1994), 33-37.

[18] Chernenko V. A., Segui C., Cesari E., Pons J. and Kokorin V. V. Some aspects of structural behavior of Ni-Mn-Ga alloys. *Journal de Physique IV,* **7,** (1997), C5/137-C5/141.

[19] Pons J., Chernenko V. A., Santamarta R. and Cesari E. Crystal structure of martensitic phases in Ni-Mn-Ga shape memory alloys. *Acta Materialia,* **48,** (2000) 3027-3038.

[20] Zheludev A., Shapiro S. M., Wochner P. and Tanner L. E. Precursor effects and premartensitic transformation in Ni_2MnGa. *Physical Review B: Condensed Matter,* **54,** (1996), 15045-15050.

[21] Cesari E., Chernenko V. A., Kokorin V. V., Pons J. and Segui C. Internal friction associated with the structural phase transformations in Ni-Mn-Ga alloys. *Acta Materialia,* **45,** (1997), 999-1004.

[22] Chernenko V. A., Segui C., Cesari E., Pons J. and Kokorin V. V. Sequence of martensitic transformations in Ni-Mn-Ga alloys. *Physical Review B: Condensed Matter and Materials Physics,* **57,** (1998), 2659-2662.

[23] Wedel B., Suzuki M., Murakami Y., Wedel C., Suzuki T., Shindo D. and Itagaki K. Low temperature crystal structure of Ni-Mn-Ga alloys. *Journal of Alloys and Compounds,* **290,** (1999), 137-143.

[24] Pons J., Santamarta R., Chernenko V. A. and Cesari E. HREM study of different martensitic phases in Ni-Mn-Ga alloys. *Materials Chemistry and Physics,* **81,** (2003), 457-459.

[25] Planes A. and Manosa L. Pretransitional Effects in Martensi tic Transformations. *Materials Science Forum,* **327-328,** (2000), 421-428.

[26] Stuhr U., Vorderwisch P., Kokorin V. V. and Lindgard P. A. Premartensitic phenomena in the ferro- and paramagnetic phases of Ni_2MnGa. *Physical Review B: Condensed Matter,* **56,** (1997), 14360-14365.

[27] Stuhr U., Vorderwisch P. and Kokorin V. V. Spin waves and phonon anomaly in the Heusler alloy Ni_2MnGa. *Physica B: Condensed Matter (Amsterdam),* **234-236,** (1997), 135-136.

[28] Stuhr U., Vorderwisch P. and Kokorin V. V. Phonon softening in Ni_2MnGa with high martensitic transition temperature. *Journal of Physics: Condensed Matter,* **12,** (2000), 7541-7545.

[29] Chernenko V. A., Pons J., Segui C. and Cesari E. Premartensitic phenomena and other phase transformations in Ni-Mn-Ga alloys studied by dynamical mechanical analysis and electron diffraction. *Acta Materialia,* **50,** (2002), 53-60.

[30] Khovailo V. V., Takagi T., Bozhko A. D., Matsumoto M., Tani J. and Shavrov V. G. Premartensitic transition in $Ni_{2+x}Mn_{1-x}Ga$ Heusler alloys. *Journal of Physics: Condensed Matter,* **13,** (2001), 9655-9662.

[31] Tsuchiya K., Yamamoto K., Hirayama T., Nakayama H., Todaka Y. and Umemoto M. TEM observation of phase transformation and magnetic structure in ferromagnetic shape memory alloys. *Electron Microscopy: Its Role in Materials Science, the Mike Meshii Symposium, Proceedings of a Symposia [held during the] TMS Annual Meeting, San Diego, CA, United States, Mar. 2-6, 2003***,** 305-312.

[32] Mañosa L., Planes A., Zarestky J., Lograsso T., Schlagel D. L. and Stassis C. Phonon softening in Ni-Mn-Ga alloys. *Physical Review B: Condensed Matter and Materials Physics,* **64,** (2001), 024305/1-6.

[33] Wu G. H., Yu C. H., Meng L. Q., Chen J. L., Yang F. M., Qi S. R., Zhan W. S., Wang Z., Zheng Y. F. and Zhao L. C. Giant magnetic-field-induced strains in Heusler alloy NiMnGa with modified composition. *Applied Physics Letters,* **75,** (1999), 2990-2992.

[34] James R. D., Tickle R. and Wuttig M. Large field-induced strains in ferromagnetic shape memory materials. *Materials Science & Engineering A,* **273-275,** (1999), 320-325.

[35] Tickle R. and James R. D. Magnetic and magnetomechanical properties of Ni_2MnGa. *Journal of Magnetism and Magnetic Materials,* **195,** (1999), 627-638.

[36] Heczko, O., Sozinov, A. and Ullakko, K. Giant field-induced reversible strain in magnetic shape memory NiMnGa alloy. IEEE Transactions on Magnetics, **36**, (2000), 3266-3268.

[37] Murray S. J., Marioni M., Allen S. M., O'Handley R. C. and Lograsso T. A. 6% Magnetic-field-induced strain by twin-boundary motion in ferromagnetic Ni-Mn-Ga. Applied Physics Letters, **77**, (2000), 886-888.

[38] Sozinov A., Likhachev A. A., Lanska N. and Ullakko K. Giant magnetic-field-induced strain in NiMnGa seven-layereded martensitic phase. Applied Physics Letters, **80**, (2002), 1746-1748.

[39] Jiang C., Liang T., Xu H., Zhang M. and Wu G. Superhigh strains by variant reorientation in the nonmodulated ferromagnetic NiMnGa alloys. *Applied Physics Letters,* **81,** (2002), 2818-2820.

[40] Sozinov A., Likhachev A. A. and Ullakko K. Crystal structures and magnetic anisotropy properties of Ni-Mn-Ga martensitic phases with giant magnetic-field-induced strain. *IEEE Transactions on Magnetics,* **38,** (2002), 2814-2816.

[41] Straka L., Heczko O. and Lanska N. Magnetic properties of various martensitic phases in Ni-Mn-Ga alloy. *IEEE Transactions on Magnetics,* **38,** (2002), 2835-2837.

[42] Likhachev A. A., Sozinov A. and Ullakko K. Different modeling concepts of magnetic shape memory and their comparison with some experimental results obtained in Ni-Mn-Ga. *Materials Science & Engineering A,* **378,** (2004), 513-518.

[43]Albertini F., Pareti L., Paoluzi A., Morellon L., Algarabel P. A., Ibarra M. R. and Righi L. Composition and temperature dependence of the magnetocrystalline anisotropy in $Ni_{2+x}Mn_{1+y}Ga_{1+z}$ (x+y+z=0) Heusler alloys. *Applied Physics Letters,* **81,** (2002), 4032-4034.

[44] Heczko O., Straka L., Lanska N., Ullakko K. and Enkovaara J. Temperature depsendence of magnetic anisotropy in Ni-Mn-Ga alloys exhibiting giant field-induced strain. *Journal of Applied Physics,* **91,** (2002), 8228-8230.

[45] Straka L. and Heczko O. Magnetic anisotropy in Ni-Mn-Ga martensites. *Journal of Applied Physics,* **93,** (2003), 8636-8638.

[46]Heczko O. and Straka L. Compositional dependence of structure, magnetization and magnetic anisotropy in Ni-Mn-Ga magnetic shape memory alloys. *Journal of Magnetism and Magnetic Materials,* **272-276,** (2004), 2045-2046.

[47] O'Handley R. C. Model for strain and magnetization in magnetic shape-memory alloys. Journal of Applied Physics, **83**, (1998), 3263-3270.

[48] Buchel'nikov V. D., Romanov V. S., Vasil'ev A. N., Takagi T. and Shavrov V. G. Model of colossal magnetostriction in the martensite phase of Ni-Mn-Ga alloys. *Journal of Experimental and Theoretical Physics (Translation of Zhurnal Eksperimental'noi i Teoreticheskoi Fiziki)*, **93**, (2001), 1302-1306.

[49] Hirsinger L. and Lexcellent C. Internal variable model for magneto-mechanical behaviour of ferromagnetic shape memory alloys Ni-Mn-Ga. *Journal de Physique IV: Proceedings*, **112**, (2003), 977-980.

[50] Heczko O., Jurek K. and Ullakko K. Magnetic properties and domain structure of magnetic shape memory Ni-Mn-Ga alloy. *Journal of Magnetism and Magnetic Materials*, **226-230**, (2001), 996-998.

[51] Sozinov A., Ezer Y., Kimmel G., Yakovenko P., Giller D., Wolfus Y., Yeshurun Y., Ullakko K. and Lindroos V. K. Large magnetic-field-induced strains in Ni-Mn-Ga alloys in rotating magnetic field. *Journal de Physique IV: Proceedings*, **11**, (2001), Pr8/311-Pr8/316.

[52] Likhachev A. A., Sozinov A. and Ullakko K. Influence of external stress on the reversibility of magnetic-field-controlled shape memory effect in Ni-Mn-Ga. *Proceedings of SPIE-The International Society for Optical Engineering*, **4333,** (2001), 197-206.

[53] De Graef M., Kishi Y., Zhu Y. and Wuttig M. Lorentz study of magnetic domains in Heusler-type ferromagnetic shape memory alloys. *Journal de Physique IV: Proceedings,* **112,** (2003), 993-996.

[54] Pan Q. and James R. D. Micromagnetic study of Ni_2MnGa under applied field (invited). *Journal of Applied Physics*, **87,** (2000), 4702-4706.

[55] Chopra H. D., Ji C. and Kokorin V. V. Magnetic-field-induced twin boundary motion in magnetic shape-memory alloys. *Physical Review B: Condensed Matter and Materials Physics*, **61,** (2000), R14913-R14915.

[56] Sullivan M. R., Ateya D. A., Pirotta S. J., Shah A. A., Wu G. H. and Chopra H. D. In situ study of temperature dependent magnetothermoelastic correlated behavior in ferromagnetic shape memory alloys. *Journal of Applied Physics*, **95,** (2004), 6951-6953.

[57] De Graef M., Willard M. A., McHenry M. E. and Zhu Y. In-situ Lorentz TEM cooling study of magnetic domain configurations in Ni_2MnGa. *IEEE Transactions on Magnetics*, **37,** (2001), 2663-2665.

[58] Park H. S., Murakami Y., Shindo D., Chernenko V. A. and Kanomata T. Behavior of magnetic domains during structural transformations in Ni_2MnGa ferromagnetic shape memory alloy. *Applied Physics Letters*, **83,** (2003), 3752-3754.

[59] Murakami Y., Shindo D., Suzuki M., Ohtsuka M. and Itagaki K. Magnetic domain structure in $Ni_{53.6}Mn_{23.4}Ga_{23.0}$ shape memory alloy films studied by electron holography and Lorentz microscopy. *Acta Materialia*, **51,** (2003), 485-494.

[60] Pan Q., Dong J. W., Palmstrom C. J., Cui J. and James R. D. Magnetic domain observations of freestanding single crystal patterned Ni_2MnGa films. *Journal of Applied Physics*, **91,** (2002), 7812-7814.

[61] Chernenko V. A., Anton R. L., Kohl M., Ohtsuka M., Orue I. and Barandiaran J. M. Magnetic domains in Ni-Mn-Ga martensitic thin films. *Journal of Physics: Condensed Matter*, **17,** (2005), 5215-5224.

[62] Soderberg O., Ge Y., Sozinov A., Hannula S. P. and Lindroos V. K. Recent breakthrough development of the magnetic shape memory effect in Ni-Mn-Ga alloys. *Smart Materials and Structures*, **14,** (2005), S223-S235.

[63] Chernenko V. A. Compositional instability of β-phase in Ni-Mn-Ga alloys. *Scripta Materialia*, **40,** (1999), 523-527.

[64] Tsuchiya K., Nakamura H., Ohtoyo D., Nakayama H., Umemoto M. and Ohtsuka H. Phase transformation and microstructures in Ni-Mn-Ga ferromagnetic shape memory alloys. *Journal de Physique IV: Proceedings*, **11,** (2001), Pr8/263-Pr8/268.

[65] Zayak A.T. and Entel P. Role of shuffles and atomic disorder in Ni-Mn-Ga. *Materials Science & Engineering A,* **378,** (2004), 419-423.

[66] Koho K., Vimpari J., Straka L., Lanska N., Soderberg O., Heczko O., Ullakko K. and Lindroos V. K. Behaviour of Ni-Mn-Ga alloys under mechanical stress. *Journal de Physique IV: Proceedings*, **112,** (2003), 943-946.

[67] Schryvers D., Boullay P., Kohn R. and Ball J. Lattice deformations at martensite-martensite interfaces in Ni-Al. *Journal de Physique IV: Proceedings*, **11,** (2001), Pr8/23-Pr8/30.

[68] Newbury D. E. Joy D. C., Echlin P., Fiori C. E. and Goldstein J. Advanced Scanning Electron Microscopy and X-Ray Microanalysis Plenum New York, (1986), 147-179.

[69] Hubert A. and Schäfer R. Magnetic domains: the analysis of magnetic microstructures Springer Berlin, (1998), 69-73.

[70] Pogany L., Ramstock K. and Hubert A, Quantitative magnetic contrast – part I: experiment. *Scanning* **14,** (1992), 263-268.

[71] Joy D. C., Leamy H. J., Ferris S. D., Yakowitz H. and Newbury D. E. Domain wall image contrast in the SEM. *Applied Physics Letters*, **28,** (1976), 466-467.

[72] Ball J. M. and James R. D. Fine phase mixtures as minimizers of energy. *Archive for Rational Mechanics and Analysis*, **100,** (1987), 13-52.

[73] Bhattacharya K. Microstructure of Martensite: Why it forms and how it gives rise to the shape-memory effect*,* Oxford University Press Inc., New York. (2003), 74-75.

[74] Hane K. F. and Shield T. W. Symmetry and microstructure in martensites. *Philosophical Magazine A: Physics of Condensed Matter: Structure, Defects and Mechanical Properties*, **78,** (1998), 1215-1252.

[75] Parpia D. Y., Tanner B. K. and Lord D. G. Direct optical observation of ferromagnetic domains. *Nature*, **303,** (1983), 684-5.

[76] Schryvers D. Microtwin sequences in thermoelastic nickel-aluminum martensite studied by conventional and high-resolution transmission electron microscopy. *Philosophical Magazine A: Physics of Condensed Matter: Structure, Defects and Mechanical Properties,* **68,** (1993), 1017-1032.

[77] Sozinov A., Likhachev A. A. and Ullakko K. Magnetic and magnetomechanical properties of Ni-Mn-Ga alloys with easy axis and easy plane of magnetization. Proceedings of SPIE-The International Society for Optical Engineering, **4333**, (2001), 189-196.

[78] Faidley L. E., Dapino M. J., Washington G. N. and Lograsso T. A. Reversible strain in Ni-Mn-Ga with collinear field and stress. *Proceedings of SPIE-The International Society for Optical Engineering*, **5761,** (2005), 501-512.

PUBLICATIONS

[P1] Söderberg O., Sozinov A., Ge Y., Hannula S.-P. and Lindroos V. K. Giant Magnetostrictive Materials. In: Buschow J (ed.) Handbook of Magnetic Materials, Elsevier Science, Amsterdam, Volume **16**, (2006), 1-39.

[P2] Ge Y., Heikinheimo E., Söderberg O. Lindroos V. K. Microanalysis of a NiMnGa alloy. Proceedings of Scandem2002, (2002), 120-121.

[P3] Ge Y., Söderberg O., Lanska N., Sozinov A., Ullakko K. and Lindroos V. K., Crystal structure of three NiMnGa alloys in powder and bulk materials. Journal de Physique IV **112**, (2003), 921-924.

[P4] Ge Y., Jiang H., Sozinov A., Söderberg O., Lanska N, Keränen J., Kauppinen E. I., Lindroos V. K. Hannula S.-P. Crystal structure and macrotwin interface of five-layered martensite in Ni-Mn-Ga magnetic shape memory alloy. Materials Science & Engineering A, **438-440**, (2006), 961-964.

[P5] Ge Y., Heczko O., Söderberg O. and Lindroos V. K. Various magnetic domain structures in a Ni-Mn-Ga martensite exhibiting magnetic shape memory effect. Journal of Applied Physics, **96**, (2004), 2159-2163.

[P6] Ge Y., Heczko O., Söderberg O. and Hannula S.-P. Direct optical observation of magnetic domains in Ni-Mn-Ga martensite. Applied Physics Letters **89**, (2006), 082502/1-3.

[P7] Ge Y., Heczko O., Söderberg O. Hannula S.-P. Magnetic domain evolution with applied field in a Ni-Mn-Ga magnetic shape memory alloy, Scripta Materialia, **54**, (2006), 2155-2160.

HELSINKI UNIVERSITY OF TECHNOLOGY DOCTORAL THESES IN MATERIALS AND EARTH SCIENCES

TKK-ME-DT-1 Ranki-Kilpinen, T.,
Sulphation of Cuprous and Cupric Oxide Dusts and Heterogeneous Copper Matte Particles in Simulated Flash Smelting Heat Recovery Boiler Conditions. 2004

TKK-ME-DT-2 Söderberg, O.,
Novel Ni-Mn-Ga Alloys and their Magnetic Shape Memory Behaviour. 2004

TKK-ME-DT-3 Kaskiala, T.,
Studies on Gas-Liquid Mass Transfer in Atmosperic Leaching of Sulphidic Zinc Concentrates. 2005

TKK-ME-DT-4 Grau, R.A..,
An Investigation of the Effect of Physical and Chemical Variables on Bubble Generation and Coalescence in Laboratory Scale Flotation Cells. 2006

TKK-ME-DT-5 Kivikytö-Reponen, P.,
Correlation of Material Characteristics and Wear of Powder Metallurgical Metal Matrix Composites. 2006

ISBN 978-951-22-8661-4
ISBN 978-951-22-8662-1 (electronic)
ISSN 1795-0074